LRP 613/98 July 1998

BEHAVIOR OF CENTRAL PLASMA RELAXATION OSCILLATIONS DURING LOCALIZED ELECTRON CYCLOTRON HEATING ON THE TCV TOKAMAK

Z.A. Pietrzyk, A. Pochelon, T.P. Goodman, M. Henderson, J.-P. Hogge, H. Reimerdes, M.Q. Tran, R. Behn, I. Furno, J.-M. Moret, Ch. Nieswand, J. Rommers, O. Sauter, W. van Toledo, H. Weisen, F. Porcelli, K.A. Razumova

Submitted for publication to
Nuclear Fusion

Behavior of Central Plasma Relaxation Oscillations during Localized Electron Cyclotron Heating on the TCV Tokamak

Z.A. Pietrzyk, A. Pochelon, T.P. Goodman, M. Henderson, J.-P. Hogge, H. Reimerdes, M.Q. Tran, R. Behn, I.Furno, J-M. Moret, Ch. Nieswand, J. Rommers, O. Sauter, W. van Toledo, H. Weisen

Centre de Recherches en Physique des Plasmas, Ecole Polytechnique Fédérale de Lausanne, Association EURATOM-Confédération Suisse, CH-1015 Lausanne, Switzerland

F. Porcelli

INFM and Politecnico di Torino, 10129 Torino, Italy

K.A. Razumova

RRC Kurchatov, 123182 Moscow, Russian Federation

I. Abstract

During initial studies of Electron Cyclotron Resonance Heating (ECRH) in the TCV tokamak, non-standard central MHD activities - such as humpbacks, saturated and inverted sawteeth - have been observed while changing the heating location, the ECRH power, the plasma shape and the safety factor. For edge safety factors $q_a > 4.5$, safety factor on axis $q(0)<1$ and small plasmas, complete sawtooth stabilization was achieved with the present 1 MW gyrotron power and it is likely that sawtooth stabilization can be achieved for all conditions at higher ECRH power. The conditions under which the various relaxation activities are produced or suppressed are reported and the origins for such non-standard behavior are discussed.

II. Introduction

ECRH is characterized by direct heating of electrons and very localized power deposition. This gives specific advantages over other plasma heating methods in which the energy is delivered less locally.

ECRH and electron cyclotron current drive (ECCD) – launching waves with a component of **k** along the toroidal magnetic field – have been studied extensively (e.g. see the review article by Erckmann and Gasparino[1]) and have been used on several machines, for example: T-10[2], WT-3[3], DIII-D[4], RTP[5],TFR[6]. Since local changes in the temperature during heating affect the current density profile, ECRH can provide current modification, just as the additional power input during ECCD can provide substantial heating.

It is to be expected that a modification of the current density profile will affect the MHD properties of the plasma. Since the localization (and therefore the current profile modifications) is different for the two methods, the resulting effects can also be different. This paper presents an analysis of the central MHD relaxation phenomena observed during initial studies on TCV using ECRH, meaning that the microwaves are launched perpendicular to the toroidal magnetic field only.

The remainder of the paper is organized as follows: after the TCV tokamak, heating system and relevant diagnostics are briefly described, in **section III**, a classification and description of the various x-ray intensity traces observed in TCV is given in **section IV**. **Section V** discusses the MHD response to variations in the localized power deposition (plasma - magnetic field - beam launch conditions) and **section VI** presents details of the electron temperature behavior during sawteeth. Possible explanations for the various types of sawtooth shapes are discussed in **section VII**. Optimization of the heating with respect to resonance location is described in **section VIII.** And conclusions are summarized in **section IX**.

III. Experimental Set-up

The TCV tokamak (Tokamak à Configuration Variable)[7] is a tokamak with vacuum vessel elongation $\kappa \equiv b/a = 3$, major radius $R = 0.9$ m, minor radius $a = 0.25$ m and maximum vacuum magnetic field $B_\phi = 1.45$ T at the chamber axis. The machine is equipped with 16 independently-controlled poloidal-field coils allow the production of plasmas with various elongations ($\kappa \sim 1$ to 2.58 achieved), negative and positive triangularities ($\delta \sim 0.7$ to 1) and plasma positions in the vessel. All of these parameters can be changed independently during a shot. This provides a very flexible tool for the study of shaped plasmas. The vessel is 65% covered with carbon tiles and is routinely boronized.

The ECRH system on TCV[8] will include six 82.7 GHz, 500 kW, 2 s gyrotrons (3 MW total) for second harmonic "X2" absorption and three 118 GHz, 500 kW, 210 s gyrotrons (1.5 MW total) for third harmonic "X3" absorption (Although the pulse length of TCV requires only 2 s pulse length, the 118 GHz gyrotron is also designed for operation at CEA, Cadarache who require the longer pulse lengths).

The system has been designed to provide maximum coupling to the wide variety of TCV plasmas. By the appropriate choice of antenna ports, good accessibility and absorption are ensured. The X2 launching antenna is capable of aiming in the poloidal and toroidal directions to cover X-mode heating, current profile modification, current drive and breakdown, see **Fig.** 1(a) and (b). The microwave beam can be swept up to 48° in a given plane in 0.3 s (thus, several times during a discharge). The orientation of the sweeping plane can be rotated

0–360° between shots; for example, to introduce a toroidal angle. In the present paper, pulses of 1.0 s at 500 kW or 0.6 s at 1.0 MW have been used.

Soft x-ray diagnostics provide the most direct information on the central MHD activity with good time resolution.

i. Four vertically-viewing, fast, soft x-ray diodes (sampling rate 250 kHz, 50 μm Be-foil filter) located at R=0.84 m, in four toroidal positions, provide measurement of MHD activity with high time resolution.

ii. 180 soft x-ray diodes (47 μm Be-foil filter), distributed in 9 cameras in one poloidal cross section, provide local soft x-ray emissivity with good spatial resolution - grid size of 3.5 cm - after tomographic reconstruction (Minimum Fisher method) with reduced temporal resolution (sampling rate 10 kHz).

iii. Four additional, vertically-viewing, soft x-ray diodes (50, 100, 250 and 650 μm Be-foil filter) located at R = 0.88 m are used to estimate the soft x-ray temperature of the plasma using the two-foil method (see below).

The Singular Value Decomposition (SVD) method[9] is used to determine the inversion radius from the tomographic data. This was compared, for several cases, with a simpler method - i.e. looking for x-ray emissivity contours (after tomographic inversion) which do not change in time during the sawtooth crash. The agreement between these two methods is ~1 cm for both the vertical and horizontal directions. The error in the determination of the inversion radius is estimated to be typically about 1.5 cm. The inversion radius is often assumed to be close to the $q(R,z) = 1$ radius; however, the difference between these two radii can be large (see Appendix B).

If the electron distribution function is Maxwellian, the ratio of the signals from two differently-filtered diodes provides a measure of the temperature. The 4 foils listed in *iii*, above, are essentially high-pass energy filters with -3 dB cut-offs at 1.9, 2.5, 3.3 and 4.5 keV, respectively. The high energy cut-off, due to the diode thickness, is the same for all filter - diode combinations. Two different ratios are calculated to provide a reasonable sensitivity over a large temperature range. Using the two foils of 50 and 250 μm, the lower part of the energy distribution is measured: the ratio of the 100 and 650 μm foil signals weights the measurement to the higher energy portion of the Bremsstrahlung distribution. In this way, good time resolution of the temperature is provided; albeit, with limited accuracy due to the assumptions inherent in the two-foil method[10].

Repetitive Thomson scattering (Nd:YAG laser at 20 Hz) is used for the electron temperature and density profile (25 point) measurements. To determine the electron density from the Thomson scattering signal, the absolute magnitude of the scattered signal is calibrated against Raman scattering from molecular Nitrogen and cross-checked for all shots by comparing the line integrated data to those obtained from one channel of the interferometer passing at the same radial (but different toroidal) location. A Maxwellian electron distribution function is assumed in the signal analysis; however, the system still provides a reliable

measurement of the temperature of the "bulk" electrons even in the presence of a high energy tail.

Plasma position and shape are determined by the LIUQE equilibrium code[11] using the input from 38 magnetic probes and the plasma pressure profiles based on the Thomson scattering measurements. These results, together with the density profiles from Thomson scattering, are used by the TORAY[12] code for the calculation of microwave beam ray-tracing and absorption. For the plasmas investigated in this paper, the TORAY code predicts close to 100% absorption for the X-mode. A non-linear (Fokker-Planck) formulation of the beam-plasma interaction may be a more accurate description[13] of the absorption; but, is not necessary for these plasmas.

Poloidal magnetic fluctuations $\tilde{b}_\vartheta$ were measured with fast (≤125 kHz sampling) pick-up coils installed inside the vacuum vessel in two toroidal arrays located in the equatorial plane: one consisting of 16 equidistant probes on the low field side (LFS) and the other 8 probes on the high field side (HFS). Fourier analysis of the signals yields toroidal mode numbers up to n=8. However, owing to the multipolar field decay $\tilde{b} \propto (r_{rs} / r_{probe})^{m+1}$ and a relatively large separation between the resonant flux surfaces r_{rs} and the probes r_{probe}, it was only possible to resolve the n=1 and n=2 components of central mode activity.

Initial ECRH experiments on TCV were performed to optimize the heating, i.e. to maximize the central temperature and confinement time, and to stabilize sawteeth. To this end, three types of *sweeps* were performed:

i. the *plasma* was swept vertically ($\Delta z \sim 30$ cm) while keeping the ECRH beam launch angle constant - thereby insuring that the beam deposition passed through both the top and bottom sides of the inversion surface along a near vertical line situated on the high field side of the magnetic axis;

ii. the *launching angle* was swept to obtained the same displacement of the power deposition relative to the plasma center while keeping the plasma at a fixed vertical height z;

iii. the *resonance location* was swept radially, by changing the magnetic field during a shot while keeping q_a constant. The beam deposition was thus varied, from 4 cm inside to 4 cm outside the high-field-side of the inversion surface.

In all three sweeps the movement was made in both directions during a shot (up ↔ down or, in ↔ out), in order to detect any possible hysteresis effect on plasma variables: no significant effect was noticed.

Although the sweeps provide a great deal of information within one discharge, they are inherently non-stationary since the absorption conditions are being changed on a time scale which is comparable to the current diffusion or current replacement times (see Appendix A). In order to distinguish between stationary and non-stationary effects, the sweeps were complemented by independent *scans,* where parameters (e.g. vertical location, launching angle

or magnetic field) where changed from shot to shot. Other scanned parameters included ECRH power, n_e, q_a, κ, and δ. Important changes on the sawtooth behavior were seen during the sweeps and confirmed by the scans. As expected, changes occurred in the temperature profile and confinement time as well.

IV. Classification of relaxation oscillations

Relaxation oscillations, characterized by the temporal variation of the soft x-ray signal, have been observed in essentially all tokamaks[14] and are attributed to the development of an n=m=1 instability on the q=1 surface. The usual (triangular shaped) sawteeth of an Ohmic plasma can acquire non-standard shapes during ECRH and/or ECCD. Names have been given to the different central-MHD features during ECRH; just as the name "sawteeth" was given originally for the resemblance to the teeth of a saw. For example, saturated sawteeth were reported in the DIII-D[15] and WT-3[3] experiments, hills were also reported in WT-3[3] when heating near q=1 on the high field side, and humpbacks were observed in the T-10[2] tokamak. All these different relaxation shapes have been observed on TCV under different shaping and heating conditions, thus, it is possible to study the relation of various heating position and plasma conditions on shapes of the MHD relaxation.

The different types of sawteeth are listed below along with their descriptions. The ordering corresponds to that in **Fig.** 2 (top to bottom). Figure 2(a) is a collection of fast soft x-ray diodes signals, measuring the line-integrated intensity along a chord passing close to the magnetic axis within the inversion radius. Figure. 2(b) shows the x-ray emissivity on the magnetic axis obtained from tomographic reconstruction for the same shots. The shapes of the line-integrated signals and the local emissivities on the magnetic axis are very similar; except for the high frequency part of the signal, missing in the tomographic reconstruction, due to the slower sampling rate.

i. *normal sawteeth* have the well-known triangular shape seen during Ohmic discharges.

ii. *partially-saturated sawteeth* have three distinct phases: a fast growth in signal after a crash, a saturation at a nearly constant level for part of the sawtooth period and, again, a growth as in a normal sawtooth until the next crash. The saturation may occur for only some sawteeth.

iii. *saturated sawteeth* lack the second growth phase of the partially-saturated sawteeth before crash.

iv. *inverted sawteeth* resemble saturated sawteeth, except that the signal decreases continuously during the saturated phase, resulting in a smaller crash.

v. *humpbacks* are increasing and decreasing emissivity hills interrupted by a crash, or crashes during the high emissivity phase. The amplitudes and the time of the crash within one humpback can change from one humpback to the next within a single plasma discharge; the rise before the crash generally differs from the rise after the crash. Humpbacks usually do not have constant period during a discharge.

vi. *hills* are similar to humpbacks without the crashes and the signal smoothly wobbles in a non-regular fashion. Therefore hills could also be called *Stabilized sawteeth* [3]. On large hills, SVD analysis of tomography shows the presence of an inversion surface, close to the expected q=1 surface, see later.

All of these relaxation phenomena may show different repetition frequencies. Sawteeth with a well defined frequency show a period of up to 10 ms during ECRH, whereas the Ohmic sawteeth period is typically 1 to 2 ms for the target plasmas used in these studies. Humpbacks have been seen with a repetition period from 10 to 110 ms in a single shot.

During a normal sawtooth, the plasma temperature generally increases, although, the temperature-rise may saturate during long sawteeth. In fact, during ECRH, with changing power deposition location, sawteeth shape may even change further or disappear completely, while plasma temperature and density remain nearly unchanged.

The values of the relevant m=1 stability parameters for TCV ECRH plasmas are given in Appendix A. The TCV discharges are in the so-called semi-collisional[16], or ion-kinetic[17] regimes. At the higher ECRH power levels projected in TCV, it will be possible to access the collisionless regime for the m=1 stability[18], as well.

Several theoretical models have been put forward[19,20,21,22] to explain the sawtooth instability. These models describe properly certain aspects of the process; however, the problem remains very complex and the physical model describing all aspects of the process is still not complete. Non-standard sawtooth behavior as observed in TCV (ii-vi, above) has not yet been theoretically addressed.

V. Central Relaxation Activity: Response to ECRH

The most significant response to a change in the heating location is the rapid change in both ***sawtooth shape*** and ***period*** as the heating location crosses the inversion radius. This effect dominates all others in the sense that very small changes in location can lead to large changes in sawtooth period, mode activity, heating and confinement. Therefore this dependence will be highlighted; then, other parameters that affect the heating such as ECRH power and plasma shape and safety factor are also discussed.

A. Dependence on heating location

Because ECRH absorption is directly related to the magnetic field strength, the heating location can be varied radially by changing the toroidal magnetic field. Such a radial sweep of the heating location during a shot is shown in Fig. 3. Note that the sawtooth behavior is the same while traversing the inversion radius from either direction (Fig. 3(a) in -> out and **Fig.** 3(b) out -> in) implying no hysteresis, as mentioned earlier. The beam heating location moves through the plasma with a velocity of about 3 cm/100 ms. A 25% increase in the sawteeth period occurs when changing the resonance location by just 1 cm, even though the

theoretical absorption layer is 1 to 2 cm thick. Figure 3(c) compares, as a function of time, the heating position with the inversion surface. The ECRH deposition crosses the inversion surface at about 0.37 s, which is near the maximum in the sawtooth period (to within a sawtooth period i.e. ~5ms -> 1.5mm). Note that there is a change of the size of the inversion radius as the heating location is moved: the inversion surface becomes largest when heating at the surface and is strongly reduced when heating outside of it.

During all sweeps in TCV the longest sawtooth periods are obtained when the heating position is near the inversion surface. The increase in sawtooth period when the heating deposition is close to the q=1 surface has already been observed in other tokamaks: e.g. DIII-D[15] ECRH experiments exhibited the longest sawteeth periods when the heating was on, or just inside, the q=1 surface and WT–3[3] sawteeth were longest when heating at the q=1 surface. As the heating location moves inside the inversion surface (by about 3 cm) there is a decrease in the sawtooth period and a transition toward saturated sawteeth. The above mentioned papers refer to heating position with respect to the *q=1 surface*. In this paper we refer to heating position with respect to the *inversion surface*, as this is directly measurable, knowing that the difference between the q=1 radius and the inversion radius may be large (see Appendix B).

The change of the sawtooth shape as the magnetic field was scanned from shot-to-shot is shown in **Fig**. 4(a). In this scan, the high field side of the inversion surface is located at R=0.825±0.015 m. The maximum sawtooth period occurs when EC power is deposited *just outside* the inversion surface, **Fig**. 4(b). Comparing magnetic field sweeps and scans, it is observed that there is no noticeable difference between the two, (the difference is well within the accuracy of the inversion surface determination), implying that the sawtooth period and shape adjust rapidly to the change in heating position.

Similar results were obtained for the vertical sweep of the plasma position, which is shown in Fig. 5. The resonance is not a straight vertical line due to the paramagnetism of the plasma. As for the B_ϕ scan, the maximum sawtooth period occurs when the heating location crosses the inversion surface, Fig. 5(b,d). (It should be mentioned here that the time of beam inversion radius crossing during up -down motion of the plasma or the beam is less accurate than during B_Φ sweep due to the error in the inversion surface curvature and the magnetic field value.) The sawtooth period behaves symmetrically for heating power deposited on either the lower or the upper portion of the inversion surfaces. However, a large discrepancy in the sawteeth shape[23,24] is observed. The up-down differences are similar those observed during co- counter- current drive experiments[25] in which the polarization was adjusted so that the x-mode fraction of the injected power varied for both the co- and counter- directions. In particular, at low x-mode fraction the co- counter-current drive efficiencies are similar to those

predicted by TORAY for the up-down positions of these experiments, respectively. And the sawteeth are also similar suggesting that the asymmetry may be related to current drive.

B. Dependence on P_{ECRH}, q_a and δ

It is of interest to investigate how changes in ECRH power, safety factor and plasma shape influence the sawteeth behavior. Three different scans are described here, beginning with the ECRH power, followed by a safety factor q_a and a triangularity δ scan.

The ECRH power dependence is shown in Fig. 6. As the ECRH power is increased the x-ray signal progresses from normal sawteeth (Ohmic - 150 kW) to partially-saturated sawteeth (440 kW), humpbacks (600 kW) and then to fully stabilized sawteeth or hills (1070 kW).

Figure 7 shows the changes in x-ray intensity during a q_a scan along with the corresponding x-ray intensities during the OH part of the discharge. The scales are the same in both parts of the figure so that a direct comparison of sawteeth amplitude and period between OH and ECRH conditions is possible. As q_a is increased, the relaxation shape changes from normal, to saturated, humpbacks and then hills - and the sawtooth period is also seen to increase.

The ECRH power and q_a scans suggest that as the overall power per unit volume within the inversion radius increases, the sawtooth type progresses from normal sawteeth through saturated sawteeth, humpbacks to hills. This is seen for the ECRH power scan with constant inversion radius but increasing power, or for the q_a scan with constant ECRH power but decreasing volume within the inversion radius, as q_a increases, see Fig. 7(b). However, as the triangularity δ is decreased from positive to negative values, the same progression is observed from normal sawteeth to saturated, inverted and then to humpbacks, see Fig. 8(a). During this progression the average inversion radius remains nearly the same, Fig. 8(b). However, due to the change in shape, the deposition moves from slightly inside to slightly outside the inversion surface. This changes the relative heating position versus the inversion surface, may effect the relaxation behavior during δ scan. Thus, both δ and q_a scans include changes in heating position relative to inversion surface position, which appears to be a major cause of sawteeth shape changes. Even though less power is deposited within the inversion radius, the sawteeth still progress from normal, to saturated, to humpbacks to hills. Therefore, there seems to be a strong dependence of sawtooth shape on plasma shaping.

C. ECRH turn-on and turn-off – relevant time scales

During the turn-on and turn-off of the ECRH pulse two distinctive time scales can easily be recognized: the time required to change from the OH x-ray intensity level to the ECRH x-ray

intensity level or vice-versa, and the time required for the sawtooth shapes to change from the normal sawteeth (during OH) to humpbacks or hills (during the ECRH pulse). Both time scales can be observed at the turn-on and turn-off of the ECRH power. However, because the gyrotron output power decays in a period shorter than 100 μs (compared to 30 ms for the turn-on to a constant power level), the turn-off is more relevant. As seen in Fig. 9, the x-ray intensity level changes from the ECRH to OH level over a period of 25–50 ms, which is consistent with the current redistribution time calculated for a constant plasma current[26]. The second time scale - the time for changing the sawtooth shape - is much shorter: the first sawtooth (a normal sawtooth) occurs within 2 ms after the ECRH turn-off. The sawtooth period then gradually decreases during the decay of the x-ray intensity level. For this shot the electron energy confinement time τ_{Ee} is ~6 ms during ECRH and ~12 ms during OH, so the sawteeth period and x-ray intensity decay are not likely related to the energy transport in the plasma.

The same two time scales can be observed during an ECRH shot with hills, shown in Fig. 10. After the ECRH pulse, the x-ray intensity has decayed after about 24 ms while the first sawtooth is seen within 5 ms (within one sawtooth period at this time), contrary to DIII-D[15] experiments, where the absence of sawteeth for as long as 160 ms after ECRH termination has been observed. This suggests that different stabilization mechanisms are at place in these two machines.

In both humpbacks and large hills, an inversion surface exists, as seen in Fig. 11, which suggests that q(0) remains below unity (assuming monotonic q-profiles) in such ECRH conditions. A comparison of the inversion radius near the ECRH turn-off and during the OH phase shows that the inversion radius increases during the ECRH pulse. The fast appearance or disappearance of the humpbacks and hills, in light of the small modification of the inversion surface, implies that the *shape* is modified due to a fast process triggered by the heating itself and not a large scale current profile modification. However, the slow change of sawtooth *period*, which is gradually decreasing as the x-ray intensity reaches the Ohmic level, may be due to a global current redistribution. There are several possible causes for the fast changes of the sawtooth shape from normal to humpbacks or hills, including a temperature-profile change, a current redistribution in only a small region near the inversion surface[2], or the slowing down of a fast electron population generated by ECRH. These will be discussed in Section VII.

VI. Characteristics of Sawtooth Types during ECRH

A. Experimental observations

In Section IV, the time evolution of the central soft x-ray emissivity was used to define and classify the different sawtooth types. However, the origin of the different characteristic

behaviors is not evident, since the x-ray emissivity is a function of electron temperature and density, impurity concentration and atomic properties. Furthermore, the intensity received on a diode depends on the filter thickness and on the geometry of the line of sight. Clarifying the source of the emissivity variations gives further insight into the observed time traces. In particular, the evolution of the electron temperature, which is usually assumed to play a dominant role in the change of x-ray emissivity during sawteeth, will be discussed in this section for each sawtooth type.

As usual, mode activity is seen prior to the crash. With ECRH, mode activity appears also between the crashes and is different for each sawtooth type. These differences can be caused by ECRH, since the localized heating has the potential to modify the pressure and current profiles and therefore the driving terms for MHD instabilities.

1. Normal (triangular) and partially-saturated sawteeth

The evolution of the x-ray emissivity, both two-foil soft x-ray temperatures - T_e^{high}(*100* and *650 μm Be*) and T_e^{low}(*50* and *250 μm Be*) - and the D_α signal of a partially-saturated sawtooth are shown in Fig. 12(a). There is a strong correlation between the x-ray emissivity and both electron "temperatures". Note that the difference in amplitude between the two "temperatures" - appearing with ECRH - suggests the presence of a non Maxwellian tail in the electron distribution function. As in the case of a normal sawtooth, the D_α signal rises rapidly after a crash and then drops between the crashes. Electron temperature- and density- profiles measured by Thomson scattering from a series of partially-saturated sawteeth are shown in figure 12(b); taken just before, and just after the crash, and during the plateau. They are compared to the x-ray emissivity profiles from tomographic reconstruction taken at the same times, Fig. 12(c). The temperature and soft x-ray emissivity profiles are strongly correlated, leading to the conclusion that the change in x-ray emissivity is dominated by the electron temperature change during partially-saturated sawteeth, as expected from analysis of normal sawteeth. This correlation is no longer present in the sawtooth types shown below.

For both normal and partially-saturated sawteeth, the D_α signal shows a peak after the crash, which indicates the loss of particles and/or energy related to outward propagation the heat pulse. Between the crashes, the D_α signal decreases, unless a saturation of the x-ray signal occurs. During these saturated phases, the D_α signal increases slightly; again suggesting increased losses.

The saturation of the x-ray emissivity is likely caused by mode activity (Fig. 13(a)), which starts to grow quickly as the x-ray emissivity flattens, then saturates. This mode has n=m=2 structure and usually decays with the end of the x-ray emissivity saturated phase giving way to an n=m=1 mode which precedes the crash. This mode is not visibly different than the Ohmic sawtooth precursor. It grows typically over several hundred microseconds until the crash and then decays on a similar time scale. The higher harmonic (n=2) of lower amplitude is

also present; although, the amplitude is still usually greater than during the saturated phase (Fig. 14(b,c)).

2. Saturated and Inverted Sawteeth

The evolution of the electron temperature and of the x-ray intensity in inverted sawteeth are plotted with respect to the time of the preceding sawtooth crash (Fig. 15). In spite of the large dispersion in the temperature data (Fig. 15b), it is clearly visible that after the crash T_{e0} saturates, or even increases, while the central x-ray emissivity decreases. Therefore, the change in T_{e0} is not responsible for the decrease of the x-ray emissivity.

As in partially-saturated sawteeth, the saturation of the central x-ray emissivity which follows the fast reheat phase, is accompanied by MHD activity (see Fig. 13(b)). It may degrade the confinement and be the reason for a slower reheat. Again, the activity has an n(=m)=2 component (4 x-ray diode analysis) which is coincident with the x-ray emissivity roll-over and is normally followed by an n=m=1 mode. The n=m=1 mode is also visible from the magnetic data and does not decrease until the crash. It is not always possible to distinguish between saturation amplitude and crash precursor amplitude (Fig. 13(b,c)).

3. Humpbacks

For humpbacks, an even stronger discrepancy between x-ray emissivity and central electron temperature is observed. Figure 16 compares the x-ray temperatures T_e^{high} and T_e^{low}, x-ray intensity, and D_α signals for a series of humpbacks. During the reheat phase of the first hump (until the crash), both x-ray "temperatures" and the x-ray emissivity increase and the D_α signal decreases. Following the crash, however, the rise in T_e^{low} is not as pronounced as the rise in x-ray intensity; and T_e^{high} decays on a longer time scale than T_e^{low}. The Thomson profiles taken from various phases of a humpback are shown in Fig. 16(b) and the corresponding x-rays profiles in Fig. 16(c). (There were no Thomson profiles during a humpback crash for this shot, so the temperature behavior at the crash is unknown.) There is no significant variation in the Thomson density profile during the humpback: all profiles are hollow in the center during the ECRH pulse (see Fig. 16(d)). Thus, a density change is not the cause of the discrepancy.

The present understanding of the electron temperature evolution during a humpback is sketched in **Fig.** 17. T_{e0} increases during the first rise of the x-ray signal and decreases rapidly at the crash; but, the magnitude of the temperature drop remains uncertain, since no Thomson measurement was available at the bottom of the crash. Following the crash, T_{e0} increases to the plateau level where it remains nearly constant until the rise of the next humpback. In contrast, the x-ray emissivity after the crash rapidly increases, then decreases slowly to the plateau level arriving at the same time as the temperature. Between the crash and the arrival at the plateau,

there may be an excess of x-ray radiation (marked as a dashed area in **Fig.** 17) over the Maxwellian Bremsstrahlung radiation, which is related to the difference between T_e^{high} and T_e^{low}.

The second hump is also accompanied by MHD activity (**Fig.** 13(c)). Oscillations of an n=(m=)2 mode are starting at the rollover of the x-ray signal, and decaying to the beginning of the plateau phase. At the same time the D_α signal shows a peak. No mode activity is observed during the plateau. The crash precursor (n=1) becomes small and is often not detectable.

4. Hilling activity

During hilling activity no correlation between T_{e0}, density, central pressure or electron energy and x-ray intensity has been found. Possibly this is due to the low level of the x-ray intensity modulation of hills. So far it is not known which combination of temperature, density, Z_{eff} or electron distribution function produces the characteristic hills in the x-ray signal. There is also no mode activity observed. Since hills occasionally evolve from humpbacks by a decrease of the crash amplitude to zero, they can be also referred to as stabilized sawteeth. On large hills SVD still shows an inversion surface, which is larger than the OH inversion surface during an earlier portion of the same shot; suggesting that for these shots, q(0)<1 and the sawteeth stabilization is due to low shear near the q=1 surface.

5. "q=2 humpbacks"

During some of the shots in which the microwave beam (i.e. antenna mirror) or the magnetic field were swept (vertical or radial motion of the heating location, respectively), humpbacks appear twice during the sweeps while moving out in normalized radius: the first occurrence when the power deposition crosses the inversion radius; and a second time when the power deposition occurs further away from the plasma center (see Fig. 18) near the q=2 surface. The change in the sawtooth period for such a sweep is shown in Fig 19(c). In the time interval t=0.55–0.6s, sawteeth are fully stabilized, Fig 19(a). The location of rational surfaces are determined from the LIUQE code. The humpbacks are very large when the power is deposited near the q=1 or q=2 flux surfaces and sawteeth are small or non-existent when the power is deposited between these surfaces.

Figure 19(b) indicates how the inversion radius is modified as the heating location is varied. The inversion radius is largest when the power deposition is crossing it from inside (0.45s), then it shrinks before the sawteeth disappear at t=0.55s preventing its further determination. When the humpbacks reappear at t=0.65s, the inversion radius is larger than before they disappear at =0.55s, but smaller than at t=0.45s. Note, however, that the inversion radius remains close to the LIUQE estimated q=1 radius.

Reconstructed x-ray emissivity contour plots of these sawteeth are shown in Fig. 18(c) and (d). There is no significant difference in MHD activity found in these two heating positions. Although there is no noticeable difference in the shape of humpbacks when heating near q=1 or near q=2, the difference in central temperature is about 1 keV. The T_{e0} is higher for q=1 heating, and the temperature profile is more peaked than for heating near the q=2 surface.

B. Generalized Description of Sawteeth

Summarizing, we define a generalized sawtooth shape, dividing a single sawtooth into three separate regions having different temperature behaviors: after the crash, the temperature increase (τ_I) terminating in a plateau region (τ_{II}) and is followed by a second temperature increase (τ_{III}). The termination of the first increase is most likely related to the appearance of an n=2 mode (see Fig. 14). However, the mode is not always *detectable* at the start of the plateau and may only be visible a little later. This mode usually decreases and disappears before the second temperature increase. The second increase in temperature is not always smooth and often starts after a mini-crash. The sawtooth crash is usually preceded by an n=1 precursor.

Within this schematic description of the different phases of a sawtooth period, the following statements hold:

i. *Normal sawteeth* do not have a plateau: $\tau_{II} = 0$,
ii. *Saturated and inverted sawteeth* do not have a second temperature increase: $\tau_{III} = 0$,
iii. *Partially-saturated sawteeth and humpbacks* consist of all three phases.

For non-standard sawteeth, i.e. humpbacks and inverted sawteeth, there is also a source of "excess" x-ray emission (see Fig. 17) (relative to the emissivity expected from the change in temperature alone). The higher emissivity may be due to a non-thermal tail in the electron distribution function. As described in section III, two temperature estimates, T_e^{high} and T_e^{low}, are made using the two-foil method. The presence of a tail is inferred from the difference between these two estimates (Fig. 16a): That is, prior to the crash this difference is not significant – consistent with a near thermal distribution – while after the crash, the thicker foil-pair (higher energy) shows a temperature in excess of that of the thinner foil-pair. The decay time-constant of the temperature difference is about 2 ms, which corresponds to the slowing-down time of a $W_e \sim 20$ keV electron tail (the thermal electron and ion temperatures are $T_e \sim 2$ keV and $T_i \sim 300$ eV, respectively).

There are two possible explanations for the observed fast electron behavior. The energetic electrons may be generated by the sawtooth reconnection process itself, which in TCV

would take place in nearly collisionless regimes (see Appendix A), favoring the formation of runaways during the crash. Evidence of fast electrons created by the sawtooth instability was observed before in JET [27]. Another possibility is that fast trapped electrons created by ECRH could decouple from the plasma bulk during the sawtooth crash, creating a distorted electron distribution function, as suggested in Ref. [28]. The decoupling condition is $\tau_d < \tau_{crash}$, where τ_d is the toroidal procession time of trapped banana orbits and τ_{crash} is the sawtooth crash time. Note that $\tau_d \propto W^{-1}$. For an electron tail of We ~ 20 keV and TCV parameters, τ_d ~100μs; therefore, the inequality $\tau_d < \tau_{crash}$ is only marginally satisfied.

If the distorted electron distribution function is created at each sawtooth crash by either of these two processes, this distorted equilibrium can produce radiation in excess of Bremsstrahlung radiation. A similar situation was observed before in cyclotron radiation in the infrared range in tokamaks[29].

VII. Discussion

A. Differences of x-ray and electron temperature behavior

During normal and partially-saturated sawteeth, the change of the electron temperature is the dominating source of the change in x-ray emissivity; however, during humpbacks and inverted sawteeth this is no longer the case. For example, the x-ray emissivity is dominated by the electron temperature before the humpback crash, while after the crash, the x-ray emissivity rises to larger value than expected from the electron temperature (Fig. 16a). The source of additional x-ray radiation could be due to a *change of the electron distribution function* triggered by the crash. This change of distribution function may create radiation above the single-temperature electron-ion Bremsstrahlung radiation of a Maxwellian plasma.

The Bremsstrahlung radiation assuming Maxwellian distributions for the electrons and ions is a function of density, Z_{eff}, and temperature $I_{SX} = \frac{n_e^2 Z_{eff}}{\sqrt{T_e}} e^{\frac{-E}{T_e}}$, and for diodes with filters, can be approximated by $I_{SX} \approx n_e^2 Z_{eff} T_e^{\alpha}$[30]. The exponent α depends on the temperatures measured and filters used and for our conditions with carbon as a dominant impurity α is close to one. Thus, there are three possible sources of I_{SX} variation. As we have seen in Chapter VI, for inverted sawteeth and humpbacks there is no similarity between the temperature and x-ray traces, and Fig. 16d shows that the density does not change before and after crash. This was also verified from the interferometer. The final source from the above equation is the Z_{eff}.

We do not have a good global measurements of Z_{eff} at this time. The electron density is low in these shots and the Z_{eff} cannot be measured from visible or infrared radiation with the present system. The lines measured in the USX range did not show changes during humpbacks or inverted sawteeth. Moreover, the change of emission during humpbacks and inverted sawteeth occurs in the plasma center without any visible indication of changes near the plasma edge, Therefore, it appears that Z_{eff} is an unlikely candidate for the difference between the humps; particularly since the experiments indicate that the difference is triggered by a internal instability in presence of the ECRH. Thus, it is suggested that the increased x-ray emission during humpbacks and inverted sawteeth can be considered as exceeding Bremsstrahlung radiation of Maxwellian plasma. This excess could be either undetected line radiation in the x-ray wavelength, or a change of the electron distribution function. Line radiation is very unlikely for the same reason as Z_{eff} and it is even more difficult to imagine excitation of the existing ions in the plasma center by a combination of ECRH and an internal instability. Thus, the most likely candidate for excess radiation in humpbacks and inverted sawteeth is a change in the distribution function of the electrons during a sawtooth crash in the present of ECRH. A difference in the distribution function of electrons between the two humps in a humpback is thus inferred by the observed difference in two x-ray "temperatures".

Non-standard sawtooth behavior during ECRH and ECCD has already been observed in other tokamaks. In particular, humpbacks were observed for the first time during ECCD experiments in T-10 [31], where it was suggested that they could be associated with the formation of reversed magnetic shear in the central plasma region, with $q(0)>1$ and $q_{min}<1$[29]. However, in TCV, humpbacks are observed during ECRH, where the amount of non-inductive current drive is relatively small and the formation of inverted shear is less likely. Humpbacks or hills could also be resulting from stabilization due to a fast ion tail. Fast ions[32]in JET[33], TFTR[34] produced "monster" sawteeth with characteristic temporal traces of central temperature, x-ray emissivity etc. However, the observed traces in TCV during sawtooth stabilization appear of somewhat different nature. In fact, the ion tail temperature is measured to be only E_i~2 keV (see Fig. 20), and this does not satisfy one of the necessary criteria for fast ion stabilization [32], i.e. $E_i/T_i>2R/r_1$.

Humpback sawteeth exhibit the peculiar feature of a second emissivity hump, whose origin has not been clearly identified. An explanation based on an impurity influx can be ruled out since no noticeable rise in Z_{eff} was observed within the measurement accuracy during the second hump; moreover, the source of x-ray emission is in the center of the plasma, with no related intensity rise on the outer surfaces as would be expected in the case of an impurity influx from the edge. A more likely explanation of the second emissivity hump is associated with the fast electrons tail created by the ECRH, or by the sawtooth crash in presence of ECRH. The stronger absorption of the microwaves by energetic electrons in the tail may enhance the non Maxwellian feature of the distribution function, and the rise in the x-ray emissivity after the

crash could be due to the relaxation of the high energy tail. In addition, a high energy electron tail could provide a local current modification near the inversion surface and occur on the fast time scales needed to support the fast transition seen at the shut-down of the ECRH (Fig. 9 and 10).

Although the temperature measured by Thomson scattering is considered as a more accurate representation of the electron temperature it is measured only every 50 ms. The x-ray temperatures can be measured on a faster time scale. Since the difference between T_e^{high} and T_e^{low} gives an idea of the change in the electron distribution function, for further analysis we will concentrate on this difference; realizing that the absolute values of the temperature may not be correct. A comparison of T_e^{high} and T_e^{low} is shown in Fig. 12 and 16 for shots with partially-saturated sawteeth and humpbacks: the x-ray intensity and the D_α signal are also shown. For both sawtooth types, $\Delta T_e = T_e^{high} - T_e^{low}$ at the sawtooth crash was negligible during the Ohmic phase and increased at the onset of ECRH indicating the possibility of a non-Maxwellian electron distribution function with a high energy tail generated by ECRH. For the partially-saturated sawteeth (Fig. 12) there is a strong correspondence between the x-ray emissivity and both electron "temperatures". By contrast, for the humpbacks, there is little correspondence between the two "temperature" signals (Fig. 16). The high energy electron tail which, upon deceleration, produces an increase in the x-ray emissivity could be at work for all types of sawteeth during ECRH, however, it is strongest during humpbacks.

B. Specific case: humpbacks generated by heating at the q=2 surface

Two possible explanations for the occurrence of humpbacks when the heating radius is near the q=2 surface, are mentioned in Sec. VI.A.6, above. The first involves a gradual modification of the q profile while the heating radius is scanned (see the schematic q profiles in Fig. 21) and the sawtooth activity changes. This explanation is not related specifically to the q=2 location. The second explanation calls for a special role played by the q=2 surface.

1. Modification of the q=1 surface

The first explanation is based on the clear observation that, as the heating radius is displaced outwards from the q=1 radius, the inversion radius initially shrinks (Fig. 19(b), 0.45-0.55s), leading to the disappearance of sawteeth (Fig. 19(a,c), 0.55-0.60s). This path to sawtooth stabilization clearly follows curve **b** of Fig. 22 assuming that, while the heating radius is shifted outwards, a shoulder with q>1 forms transiently in the q profile as a result of a change in the local electron temperature and resistivity profiles (see Fig. 21, 0.55s). Then, at later times t>0.65s, the q profile becomes flatter than at t=0.5s, with a larger q=1 radius, as shown in Fig. 21 for t = 0.67s. The sawtooth behavior observed in Fig.19 is *consistent* with the schematic in Fig. 21, but is only speculative, since there is no direct measurement of the

current profile. Clearly, the distance between the heating radius and the sawtooth mixing radius (see Appendix B) is not much different for the two times t=0.5s and t=0.675s. In this sense, it is not surprising that the humpbacks at these times look (from the x-rays) very similar, as shown in Fig. 18(c,d). The q=2 radius does not play any special role in this case.

2. q=2 surface effect

On the other hand, plasma stability against internal kinks in a torus can be affected by local changes near the q=2 surface[35,36]. This is due to the toroidal coupling between the m=1, n=1 component, resonant at q=1, and the m=2, n=1 component, resonant at q=2. We cannot exclude, therefore, that heating close to the q=2 surface provides a way to trigger sawteeth. This interesting possibility deserves further investigation, as it could provide an additional parameter for sawtooth control.

C. sawtooth stabilization

Two possible approaches to full sawtooth stabilization can be envisioned (Fig. 22): *a)* increasing the sawtooth period until it become 'infinite' (in practice, longer than the experiment), or *b)* decreasing the sawteeth period and amplitude to zero (below noise level). Both approaches can be realized with ECRH. The sawtooth period has been shown to increase when heating near the inversion radius and a sufficient level of ECRH may achieve full stabilization with the risk of experiencing "monster" sawteeth as the period is increased. Decreasing the sawtooth period (usually called "destabilization of sawteeth") provides a safer path to stabilization as the amplitude and period are gradually decreased by heating just outside the inversion radius, driving q(0)>1. Both of these two approaches, which can be seen in a single B_ϕ scan shot, Fig. 23, are discussed below and an explanation of the processes is provided.

During the scans in heating deposition (Fig. 4 and 5) the sawtooth period increases as the deposition location crosses the inversion radius. ECRH causes a local increase of electron temperature, which then decreases the plasma resistivity, resulting in increased current driven in the heated region by the inductive electric field which is already present in the plasma. This, in turn, affects the local shear and hence the threshold for the onset of internal kink modes[32,33,37]. A local reduction of the magnetic shear near the inversion surface can lead to a lengthening of the sawtooth period to full stabilization. Indeed, this effect was considered to be the main cause of sawtooth suppression during ECRH discharges in WT-3[3], as well as in the minority ion current drive experiment in JET[38].

Two other important factors affecting the stability of internal kinks are the average plasma pressure gradient inside the inversion radius and the presence of fast electrons. The pressure gradient drive for internal kinks is measured by the q=1 poloidal beta parameter[21,32]:

$$\beta_{p_1} = [8\pi/B^2_p(r_1)]\ [\ <p>_{r_1} - p(r_1)], \quad (1)$$

where $<p>_{r_1}$ is the volume - average pressure within the q=1 surface and B_p is the flux surface average of the poloidal field. Note that $\beta_{p_1} = 0$ for a flat pressure inside q=1. The ideal MHD drive increases with β_{p_1}; indeed, internal kinks become ideal MHD unstable for β_{p_1} above β_{crit} (typically between 0.1 and 0.3)[21,30]. When ECRH is absorbed outside of the plasma center, the pressure profiles should be flatter, which may remove a possible instability drive and lead to sawtooth stabilization. (The situation, however, is more complex, since resistive internal kinks can be unstable below the ideal MHD threshold, i.e. even at $\beta_{p_1} = 0$. Nevertheless, the further away from ideal marginal stability on the ideal MHD stable side, the more stable the resistive plasma becomes[39], and experimentally the pressure profiles change within experimental error when moving the heating from the center to the inversion radius).

We suspect that such an effect plays an important role in the lengthening of the sawtooth period and the full sawtooth suppression in TCV. A polarimeter, to be operational in the near future on TCV, could help to clarify these speculative explanations of the sawtooth stabilization at different heating locations.

The second approach to full sawteeth stabilization can be achieved by driving q(0)>1. During the sweep in B_ϕ (Fig. 3), the ECRH deposition traversed the inversion radius from inside the surface to outside (on the high field side). Once the beam deposition was outside of the inversion surface, the average inversion radius decreased and there was a corresponding decrease in the sawtooth period, see Fig. 3. Depending on the ECRH power available and the initial size of the inversion radius, one could envision shrinking the inversion surface, reducing the period and amplitude of the sawteeth, as seen in Fig. 23.

Both methods of sawtooth stabilization are seen during the sweep of the resonance location at constant q_a (the magnetic field and plasma current were varied simultaneously) , see Fig. 23, in this shot. The heating location varies from roughly the magnetic axis to a normalized radius of approximately ρ~0.75 on the high field side of the plasma. Figure 23(a) shows the evolution of central x-ray intensity and Fig. 23(b), the sawtooth period. The sawtooth period at the onset of the ECRH is approximately equal to the OH period; then increases as the heating location moves toward the inversion radius – the sawtooth shape changes from saturated to humpback. At the inversion radius, the sawtooth period reaches a maximum. (We suspect that the sawteeth would have been fully stabilized by increasing ECRH power, or if the heating location relative to the inversion surface would have been kept constant, just inside the inversion surface). As the heating location traverses the inversion radius the sawtooth period decreases, and sawteeth eventually disappear: the inversion surface is also

undetectable at this time. The LIUQE reconstruction code indicates that q(0) increased above one so sawtooth stabilization occurs with the sawtooth period going to zero. However, for shots with sawtooth stabilization and q(0)<1, the inversion surface is still clearly visible (see Fig. 11).

VIII. Optimization of resonance position with respect to heating and confinement

One of the principle objectives of the preliminary studies of ECRH on TCV was to determine the optimum heating deposition location i.e. to produce the hottest or best confined plasmas. The change in sawteeth proved to be interesting in its own right and is the primary interest of this paper. Nevertheless, optimization of heating is also discussed here since it appears likely that the sawtooth period, heating and electron confinement time are inter-related.

As shown in Section III, the optimum location for sawtooth stabilization occurs near the inversion surface. Changes in central electron temperature (T_{e0}) and the electron confinement time (τ_{Ee}) are also strongly correlated with the heating location relative to the inversion radius.

Using the scans of B_ϕ, the effect of the heating localization on each of these parameters can be studied. There were several B_ϕ scans ($1{,}29T<B_\phi<1.41T$) performed, each with different values of q_a ($2.3<q_a<6.4$) The change of the central electron temperature (T_{e0} - Fig. 24) during ECRH, relative to the OH phase, are given as a function of the distance from the inversion surface. The vertical axis, $\Delta T_{e0}/T_{e0}$, is the difference in the **central** electron temperature between the ECRH and Ohmic phases divided by the Ohmic electron temperature: $\Delta T_{e0}/T_{e0} = [T_e(0)_{ECRH}-T_e(0)_{OH}] \,/\, T_e(0)_{OH}$. The horizontal axis is the difference between the heating location and the inversion surface in major radius, measured at the vertical height of the heating. Heating is always on the HFS. There appears to be a maximum in $\Delta T_e/T_e$ when the heating deposition is near or just inside the inversion surface. As the deposition location is moved away from the inversion surface (in minor radius) the relative temperature rise between the ECRH and Ohmic phase decreases. As the deposition location moves inside of the inversion surface (toward the magnetic axis to the right in the figure) the relative temperature seems to peak at about 2 cm inside the inversion radius.

A similar analysis was performed for the electron energy confinement time plotting (τ_{Ee} - Fig. 25), $\Delta\tau_{Ee(ECRH)} \,/\, \tau_{Ee(OH)} = [\tau_{Ee(ECRH)} - \tau_{Ee(OH)}] \,/\, \tau_{Ee(OH)}$,this yields the variation of degradation in the electron confinement time as a function of the localization of heating. This shows that confinement time degradation is not much different in the when the heating deposition is anywhere inside of the inversion surface. As the deposition traverses the inversion outward (in minor radius), the confinement time is increasingly degraded.

It appears that an optimum in sawteeth stabilization and central electron temperature occurs when heating just inside the inversion surface. Furthermore, minimal power degradation

of the electron energy confinement time occurs when heating anywhere inside of the inversion radius. Therefore, to maximize at the same time the central electron temperature, the confinement time and the sawteeth period, heating deposition should be placed just inside of the inversion radius.

IX. Conclusions

Localized heat deposition with ECRH strongly influences sawtooth activity in the TCV plasma. The sawtooth period and the sawtooth shape, as seen on the soft x-ray signals, depend strongly on the deposition radius relative to the sawtooth inversion radius. The sawtooth period is maximized with a deposition close to the inversion radius and shows values similar values regardless to the position explored (above, below or on the HFS of the magnetic axis). This invariance of a sawtooth period is not found for the sawtooth shape. The sawtooth shape, with heating off axis changes when heating moves from upper to lower part of the inversion surface. Above a certain ECRH power the sawteeth may disappear when heating near the inversion surface, leaving only hilling activities. As the sawtooth period and MHD activity are dependent on triangularity in OH plasmas[40], sawtooth stabilization by ECRH is also influenced by negative plasma triangularity.

Changing up-down heating position on the inversion surface does not change sawteeth period but changes their shape. That indicates that shape and period do not depend on the same variables. It appears that the period is most likely a function of the shear near the inversion surface, while the shape may depend on the amount of a small current driven in co- or counter-direction at that surface[24].

Two approaches to sawteeth stabilization are possible. In one approach, the sawtooth period is driven to times longer than the duration of the plasma discharge; in the second approach, the sawtooth period is decreased to zero. With the ECRH the first method is used by heating just inside the inversion radius and the second method, by heating outside of it. Increasing the sawtooth period produces large sawteeth, which can be undesirable, however stabilization is obtained with a very efficient heating, good confinement time, high central electron temperature. Diminishing the sawtooth period a safer approach to sawteeth stabilization, but the heating position is not the optimum for energy confinement and plasma performance may be lower.

All the different sawteeth shapes seen on the x-ray emissivity are not as different as seen by the central temperature behavior. As can be deduced from the Thomson scattering and x-ray temperature data during ECRH, the temperature rapidly increases after a sawtooth crash, then saturates, most likely due to n=2 mode, and sometimes increases again before the following crash. The different x-ray relaxation shapes are related to the length of the "plateau", the

increase temperature before the crash and the amount of excess radiation after crash. For all sawtooth shapes, the (1,1) mode is visible as a precursor. This suggest that all of the sawtooth crashes are due to the same instability. However, the different plasma conditions, or geometrical heating conditions and perhaps the different amount of fast non-thermal electrons creates the different shapes.

An excess of x-ray emissivity in humpbacks and inverted sawteeth has been found after crash during ECRH, when heating near the inversion surface. This excess may be caused by a de-coupling of high and low energy electrons during the sawtooth crash producing a non-thermal electron distribution function, or it may be created by the sawtooth crash. In both cases the effect would be enhanced by the present of ECRH with stronger absorption of wave energy by energetic electron. Non thermal electrons would radiate energy in addition to equilibrium Bremsstrahlung radiation.

The reason for the temperature increase before the crash in partially-saturated sawteeth and humpbacks is still not completely clear. The measured n=2 mode apparently responsible for the sawtooth saturation seems to decay during plateau phase, but n=1 mode is present during the temperature rise before the crash with a comparable amplitude. There is clear difference in effect of n=1 and n=2 modes on a temperature behavior, but not a clear physical picture why there should be a difference. There may also be modes with higher mode numbers present which could affect the temperature strongly, but these modes could not be detectable neither on the x-ray nor on magnetic diagnostics in the present experimental conditions.

During some of the shots with a sweep of the heating location humpbacks with long periods were observed for heating at two clearly different radial locations. The most distant location from the axis leads to so called "q=2 humpback", because these humpbacks are produced when heating near the **calculated** q=2 surface. These effectively may be caused by the vicinity of q=2 surface (mode interactions) or may alternatively be due to a strong migration of the q=1 surface from the inversion surface (see Fig. 21 and Appendix B).

X. Acknowledgments

The authors thank all the TCV team for a help this study. This work was partially supported by Swiss National Science Funds. F. Porcelli was supported in part by the Italian National Research Council (CNR).

XI. Appendices

A. *TCV Parameters*

It is of interest to ascertain the relevant collisionality regime for the m=1 instability in TCV. Values of the relevant internal kink instability parameters in ECRH TCV discharges are listed in Table 1 (parameter range: $1.2 < n_e(0) < 3 \;\; 10^{19} m^{-3}$, $1 < T_e(0) < 4$ keV). The appropriate regime for m=1 stability studies in these discharges is the so-called semi-collisional[17] or ion-kinetic regime[18], just like large size, high power tokamaks, in spite of the relatively small dimensions of TCV. The ion-kinetic regime is defined by the inequalities: $\rho_i > \delta_\eta > d_e$ where, ρ_i is the ion Larmor radius, $\delta_\eta = S^{-1/3} r_1$ is the resistive kink layer width[41], d_e is the inertial skin depth, S is the magnetic Reynolds number and r_1 is the radius of the inversion surface. Diamagnetic frequency effects also play an important role on stability, as $\nu_{ei} > \omega^* > \gamma_\rho$, where ν_{ei} is the electron ion collision frequency, ω^* is the diamagnetic frequency and γ_ρ is the characteristic semi-collisional growth rate[18]. At the highest ECRH power and temperature on TCV we will be able to access the collisionless regime for m=1 stability; in this regime $d_e > \delta_\eta$ and ν_{ei} is smaller than the linear growth rates[19].

Table 1. Reference ECRH plasma values in TCV

Alfvén time	$\tau_A = \sqrt{3}R/V_A$	0.2 - 0.3	μs
Resistive diffusion time	$\tau_\eta = 4\pi r_1^2/\eta_{\parallel} c^2$	160 - 430	ms
Current replacement time[26]	$\tau_\eta^* = \frac{1}{6}\mu I_p R_0 / V_s$	30-70	ms
Sawteeth period (measured)	τ_{ST}	2 - 110 - ∞	ms
Magnetic Reynolds number	$S = \tau_\eta / \tau_A$	0.5 - 2 10^6	
Inversion surface (measured)	r_1	4 - 12	cm
Ion Larmor radius	ρ_i	0.2 - 0.3	cm
Resistive kink layer width	δ_η	0.03-0.12	cm
Electron inertial skin depth	$d_e = c/\omega_{pe}$	0.1	cm
Semi-collisional m=1 growth rate	γ_ρ	0.1 - 0.2 10^5	s^{-1}
Diamagnetic frequency	ω_*	0.2 - 3 10^5	s^{-1}
Electron collision frequency	ν_{ei}	2.5 - 5 10^5	s^{-1}

B. *Analytical relationship between the inversion radius and the q=1 radius*

In this Appendix, we argue that the $q=1$ radius before the onset of a resistive kink mode (leading to a sawtooth crash) and the sawtooth inversion radius, in general, do not coincide. On theoretical grounds, the difference between the two depends on the pre-crash profiles of q and temperature, and on the assumed relaxation model. This difference can be large, especially for q profiles which are rather flat in the region where $q\leq 1$ and rising quickly outside the $q=1$ radius.

In order to illustrate this from a modeling standpoint, we adopt the Kadomtsev full reconnection model in simplified cylindrical geometry[20]. This model yields the relaxed q profile, q^{rel}, as a function of the pre-crash profile, q^{pre}. One considers the helical flux function, which, for a constant equilibrium toroidal field, can be written as (omitting constant factors):

$$\psi_*^{pre}(r^2)=\int_0^{r^2}\left[\frac{1}{q^{pre}(\hat{r}^2)}-1\right]d\hat{r}^2 \qquad (B.1)$$

where, for convenience, the radial coordinate is normalized to the $q=1$ radius, i.e. $q^{rel}(1)=1$. Clearly, for a monotonic q profile, $d\psi_*^{pre}/dr^2=0$ at $r^2=1$. An example of ψ_*^{pre} is shown in **Fig**. B1.

Kadomtsev's model is based on the following assumptions:

1. All surfaces with $r^2<1$ reconnect with surfaces $1<r^2<r^2_{mix}$, where

$$\psi_*^{pre}(r_{mix}^2)=\psi_*^{pre}(0). \qquad (B.2)$$

The latter relation defines the mixing radius, r_{mix}, which is an experimentally observable quantity. The reconnection process is brought by a resistive internal kink mode, which shifts the flux surfaces with $r^2<1$, rigidly.

2. The helical flux is conserved; therefore, it can be considered as a surface label even as the surfaces reconnect. Thus, any surface $r=r_1<1$ reconnects with a surface $r=r_2$, $1<r_2<r_{mix}$, having the same helical flux, i.e. such that

$$\psi_*^{pre}(r_1^2)=\psi_*^{pre}(r_2^2). \qquad (B.3)$$

3. The toroidal flux is also conserved. For a constant toroidal field this implies that, when the reconnection process is completed, the surface, formed by the reconnection of the pre-crash radii $r=r_1$ and $r=r_2$, becomes a circle of radius

$$r^2=r_2^2-r_1^2. \qquad (B.4)$$

Conservation of the helical flux implies that:

$$\psi_*^{rel}(r^2)=\psi_*^{pre}(r_1^2). \qquad (B.5)$$

where $r_1^2=r_1^2(r^2)$ through Eqs. (B.3) and (B.4). Finally, $q^{rel}(r^2)=\left[1+d\psi_*^{rel}/dr^2\right]^{-1}$. The relaxed q profile has $q^{rel}(0)=1$ and $q^{rel}(r^2)\geq 1$ for $r^2>0$, ($q^{rel}(r^2)=1$ for $r^2<r^2_{min}$ if $q^{pre}(r^2)=1$ for $r^2\leq 1$).

Let us now consider the relaxation of the plasma density. A reasonable assumption is that particle transport across helical flux surfaces is negligible during the reconnection process. This leads to the particle conservation relation:

$$\int_0^{r^2} n^{rel}(\hat{r}^2)\mathrm{d}\hat{r}^2 = \int_{r_1^2(r^2)}^{r_2^2(r^2)} n^{pre}(\hat{r}^2)\mathrm{d}\hat{r}^2 \tag{B.6}$$

Differentiating this relation, we obtain the relaxed density profile

$$n^{rel}(r^2) = \frac{dr_2^2}{dr^2} n^{pre}[r_2^2(r^2)] - \frac{dr_1^2}{dr^2} n^{pre}[r_1^2(r^2)] \tag{B.7}$$

where again r_1^2 and r_2^2 are functions of r^2 through Eqs. (B.4) and (B.5). Note that $dr_1^2/dr^2 < 0$.

A similar relation can be obtained for the plasma pressure, except that in this case the plasma thermal energy is not constant but can be expected to increase at the expense of the magnetic energy converted during the reconnection process. If this converted energy is small, as is often the case for realistic Tokamak parameters and relatively small amplitude sawteeth, then,

$$p^{rel}(r^2) = \frac{dr_2^2}{dr^2} p^{pre}[r_2^2(r^2)] - \frac{dr_1^2}{dr^2} p^{pre}[r_1^2(r^2)]. \tag{B.8}$$

The relaxed temperature is clearly $T^{rel} = p^{rel}/n^{rel}$.

Now we can evaluate the theoretical inversion and mixing radii for two cases of interest. In the first case, both $1/q^{pre}$ and T^{pre} are parabolic in r; i.e. $T^{pre}(r^2)=T_o(1-r^2/r_T^2)$, with r_T the temperature gradient scale length normalized to the q=1 radius, while $n^{pre}(r^2)=const.$ We obtain $r_1^2=1-r^2/2$, $r_2^2=1+r^2/2$, $n^{rel} = const.$ and

$$T^{rel}(r^2)=T_o(1-r_T^{-2})=\text{const. for } r^2<r_{mix}^2, \tag{B.9}$$

where the mixing radius is in this case

$$r_{mix}=\sqrt{2}. \tag{B.10}$$

The inversion radius for the temperature profile satisfies

$$T^{rel}(r_{inv}^2)=T^{pre}(r_{inv}^2). \tag{B.11}$$

In this particular case, it coincides with the pre-crash $q=1$ radius:

$$r_{inv}=1. \tag{B.12}$$

In the second example, let us consider a parabolic T^{pre} and a constant n^{pre} as before, but now let us assume the limiting case where the pre-crash q profile is nearly flat - about unity - up to $r^2=1$, and increases rapidly thereafter. We find immediately that

$$r_{mix}=1, \tag{B.13}$$

i.e. the **mixing radius** coincides with the pre-crash $q=1$ radius in this case. The inversion radius must be smaller. Now, it is readily found that $r_2^2=1$, $r_1^2=1-r^2$, n^{rel} remains constant and $T^{rel}(r^2) = T^{pre}(r_1^2) = T_o(1 - 1/r_T^2 + r^2/r_T^2)$ for $r^2<1$. Thus, the relaxed temperature profile is

not flat in this case; rather, it increases parabolically up to $r^2=1$, where $T^{rel}(1^-) = T_o$, then jumps to the pre-crash value at $r^2=1^+$. Using Eq. (B.11), we find the inversion radius

$$r_{inv}=\frac{\sqrt{2}}{2} \qquad \text{(B.14)}$$

which is considerably smaller that the pre-crash q=1 radius.

The results above should be taken as a note of caution against assimilating the experimental inversion radius to the pre-crash q=1 radius. They should however not be considered as providing the actual relationship between the two radii (and the mixing radius), since the Kadomtsev model is a rough representation of the reconnection process which does not always adequately represent the complexity of the sawtooth reconnection process.

XII. References

1. ERCKMANN, V., GASPARINO, U., Plasma Phys. Controlled Fusion **36** (1994) 1862.
2. ALIKAEV, V.V., ARSENTIEV, Yu.I., BAGDASAROV, A.A. et al., Plasma Phys. and Controlled Nuclear Fusion Research 1984 (Proc. 10th Int. Conf. London, 1984), Vol. 1, IAEA, Vienna (1985) 419.
3. HANADA, K., TANAKA, H., IDA, M., IDE, S. et al., Phys. Rev. Lett. **66** (1991) 1974.
4. STALLARD, B.W., CONTENT, D.A., GROEBNER, R.J., HILL, D.N., et al., Nucl. Fusion **33** (1990) 2235.
5. LOPES -CARDOZO, N.J., HOGEWEIJ, G.M.D., DE BAAR, M. et al., Plasma Physics Controlled Fusion **39** (1997) B303.
6. TFR Group, FOM/ECRH Team, Nucl. Fusion **28** (1988) 1995.
7. HOFMANN, F., LISTER, J.B., ANTON, M., et al., Plasma Physics Controlled Fusion **36** (1994) B277.
8. GOODMAN, T.P., ALBERTI, S., HENDERSON, M.A., POCHELON, A., TRAN, M.Q., Fusion Technology, Proc. of the 19th Symp. on Fusion Technology (SOFT) Lisbon 1996, **1** (1996) 565.
9. ANTON, M., WEISEN, H. et al., Plasma Physics Control. Fusion **38** (1996) 1849; and FURNO, I., private communication.
10. JAHODA, F.C., LITTLE, E.M., QUINN, W.E, SAWYER, G.A., STRATTON, T.F., Phys. Rev. **119** (1960) 843.
11. HOFMANN, F., TONETTI, G., Nucl. Fusion **28** (1988) 1871.
12. MATSUDA, K., IEEE Transactions on Plasma Science **17** (1989) 6; and MYER; R.C., PORKOLAB, M., SMITH, G.R., KRITZ, A.H., Nucl. Fusion **29** (1989) 2155.
13. HARVEY, R.W. et al., Phys. Rev. Lett. **62** (1989) 6.
14. von GOELER, S., STODIEK, W., SAUTHOFF, N., Phys. Rev. Lett. **33** (1974) 1201.

15. SNIDER, R.T., CONTENT, D., JAMES, R., LOHR, J., et al., Phys. Fluids B **1** (1989) 404.

16. DRAKE, J.F., ANTONSEN, T.M., HASSAM, A.B. and GLADD, N.T., Phys. Fluids **26** (1983) 2509.

17. PEGORARO, F., PORCELLI, F. and SCHEP, T.J., Phys. Fluids B **1** (1989) 364.

18. PORCELLI, F., Phys. Rev. Lett. **66** (1991) 425.

19. KADOMTSEV, B.B., Soviet Journal of Plasma Physics **1** (1976) 389.

20. PORCELLI, F., BOUCHER, D. and ROSENBLUTH, M.N., Plasma Phys. and Controlled Fusion **38** (1996) 2163.

21. LICHTENBERG, A.J., Nucl. Fusion **24** (1984) 1303.

22. WESSON, J.A., Plasma Phys. and Contr. Fusion **28** (1986) 243.

23. PIETRZYK, Z.A., POCHELON, A., GOODMAN, T.P., HENDERSON, M.A., REIMERDES, H., TRAN, M.Q., et al., 2nd Europhysics Top. Conf. on RF Heating and Current Drive of Fusion Devices, Brussels, Vol. 22A (1998) 249

24. GOODMAN, T.P., HENDERSON, M.A., PIETRZYK, Z.A., POCHELON, A., TRAN, M.Q., et al. 25th EPS Conf. on Contr. Fusion and Plasma Phys. (Combined with ICPP 1998), Praha 1998.

25. GOODMAN, T.P., HENDERSON, M., PERTHUISOT, F. PIETRZYK, Z.A. et al., 2nd Europhysics. Top. Conf. on RF Heating and Current Drive of Fusion Devices, Brussels **22A** (1998) 245.

26. MIKKELSEN, D.R., Phys. Fluids B **1** (1989) 333.

27. HUGON, M., BARTLETT, D., BRUSATI, M., et al., 19th EPS Conf. on Contr. Fusion and Plasma Phys. Innsbruck (1992) **16c** I-119.

28 HASTIE, R.J., "Change in Electron Cyclotron Emission during a Sawtooth Collapse" JET-R(94)03 (1994)

29. GANDY, R.F., HUTCHINSON, I.H., YATES, D.H., Phys. Rev. Lett. **54** (1985) 800.

30. WEISEN, H., PASINI, D., WELLER. A., EDWARDS, A.W. Rev. Sci. Instrum. **62** (1991) 1531

31. RAZUMOVA, K.A., BAGDASAROV, A.A., GORSHKOV, A.A., et al., Plasma Physics Reports **23** (1997) 13.

32. PORCELLI, F., Plasma Phys. and Cont. Fusion. 33 (1991) 1601

33. CAMPBELL, D.J. et al., Phys. Rev. Lett. **60** (1988) 2148.

34. HOSEA, J.C. et al. Plasma Phys. and Controlled Nuclear Fusion Research 1990 (Proc. 13th Int. Conf. Washington, 1990), Vol. 1, IAEA, Vienna (1991) 669.

35. BUSSAC, M.N., PELLAT, R.T., EDERY, D., SOULÉ, J.L., Phys. Rev. Lett. **35** (1975) 1638.

36. BUSSAC, M.N., EDERY, D., PELLAT, R. and SOULÉ, J.L., Plasma Phys. and Controlled Nuclear Fusion Research 1984 (Proc. 6th Int. Conf. Berchtesgaden, 1976), Vol. 1, IAEA, Vienna (1977) 607.

37. SOLTWITCH, H., STODIEK, W., MANIKHAM, J., SCHLÜTER, Plasma Phys. and Controlled Nuclear Fusion Research 1986 (Proc. 11th Int. Conf. Kyoto, 1986), Vol. 1, IAEA, Vienna (1987) 263.

38. BHATNAGAR, V.P. et al., Nucl. Fusion **34** (1994) 1579.

39. MIGLIULO, S., PEGORARO, F., and PORCELLI, F., Phys. Fluids **B3** (1991) 1338.

40. WEISEN, H. MORET, J.-M., FRANKE, S., FURNO, I., MARTIN, Y., et al., Nucl. Fusion 37 (1997) 1741.

41. COPPI, B., GALVAO, R. et al., Fiz. Plasmy **2** (1976) 961, [Sov. J. Plasma Phys. **1** (1976) 389].

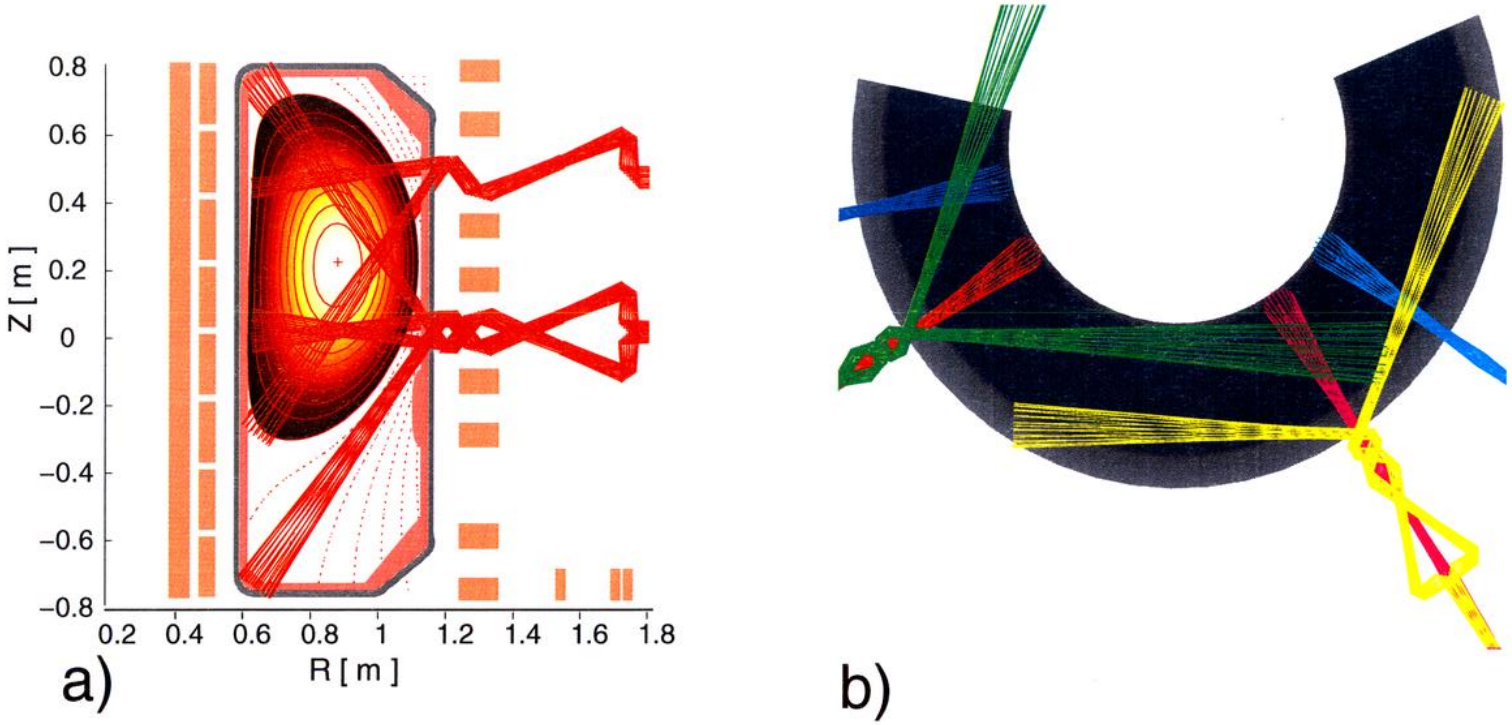

Figure 1. Accessibility of second harmonic quasi-optical launchers in the a) poloidal and b) toroidal planes. Launchers are located in equatorial port and upper lateral ports. Both upper lateral and equatorial launchers have been used.

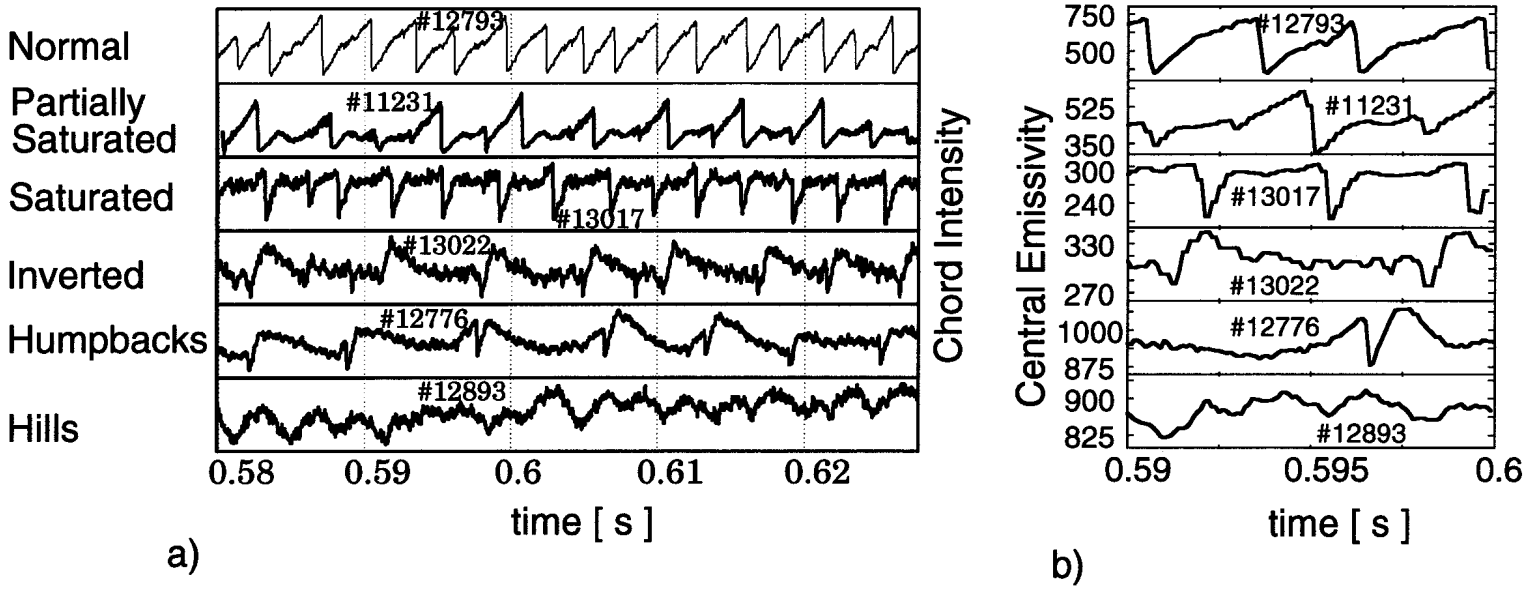

Figure 2. Different central MHD relaxation activity during ECRH as seen a) along a close to central soft x-ray line-integrated chord (250 kHz sampling) and b) on tomographically reconstructed soft x-ray central emmisivity (10 kHz sampling).

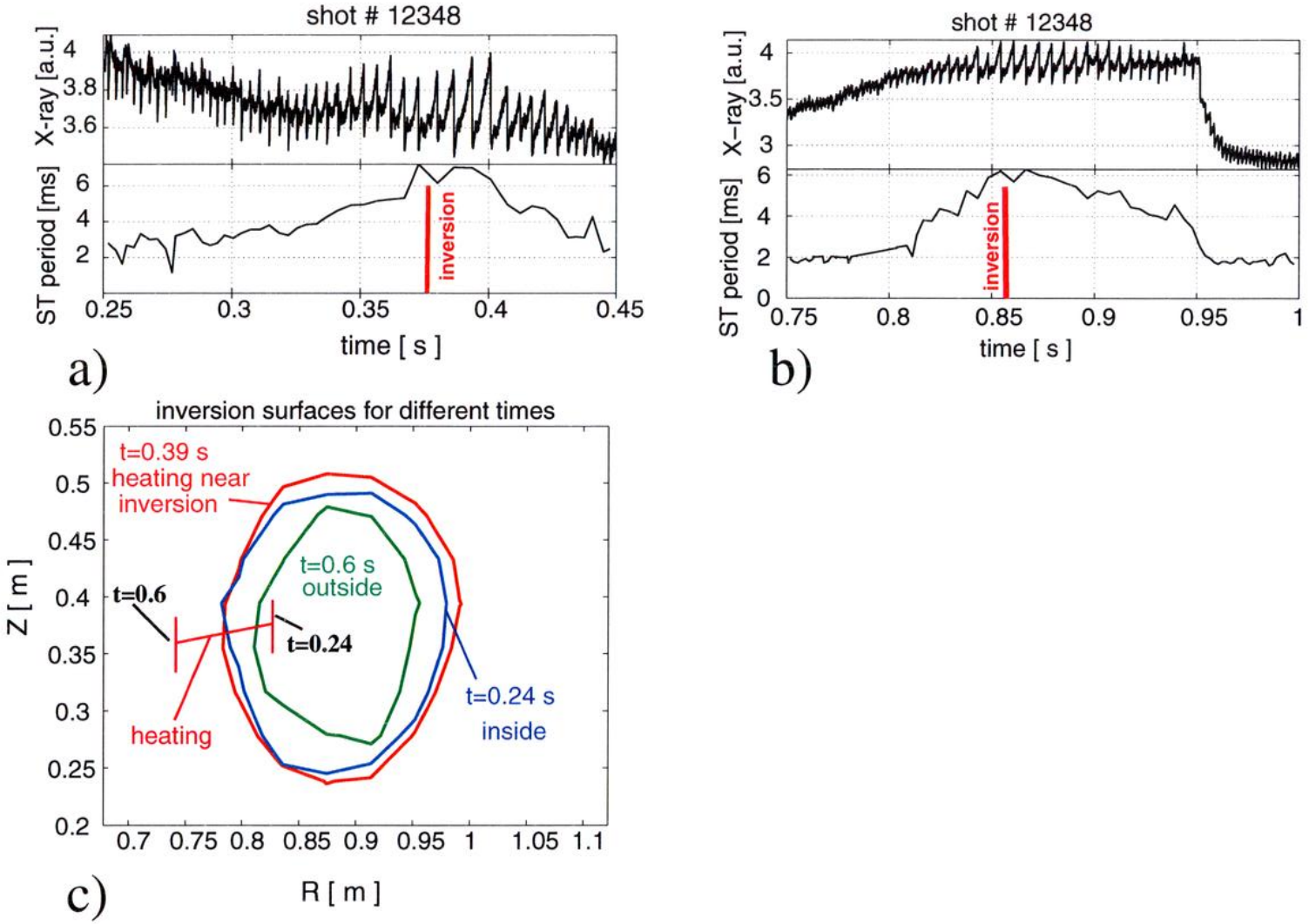

Figuge 3. Soft x-ray signal and sawteeth period versus time while the heat deposition location is crossing the inversion surface from a) outside to inside and b) inside to outside. c) Heating location and inversion surface at different times; the heating location moves at about 3 cm/100 ms (q_a=3.4, κ=1.29, $n_e(0)$=1.8 10^{19} m^{-3}).

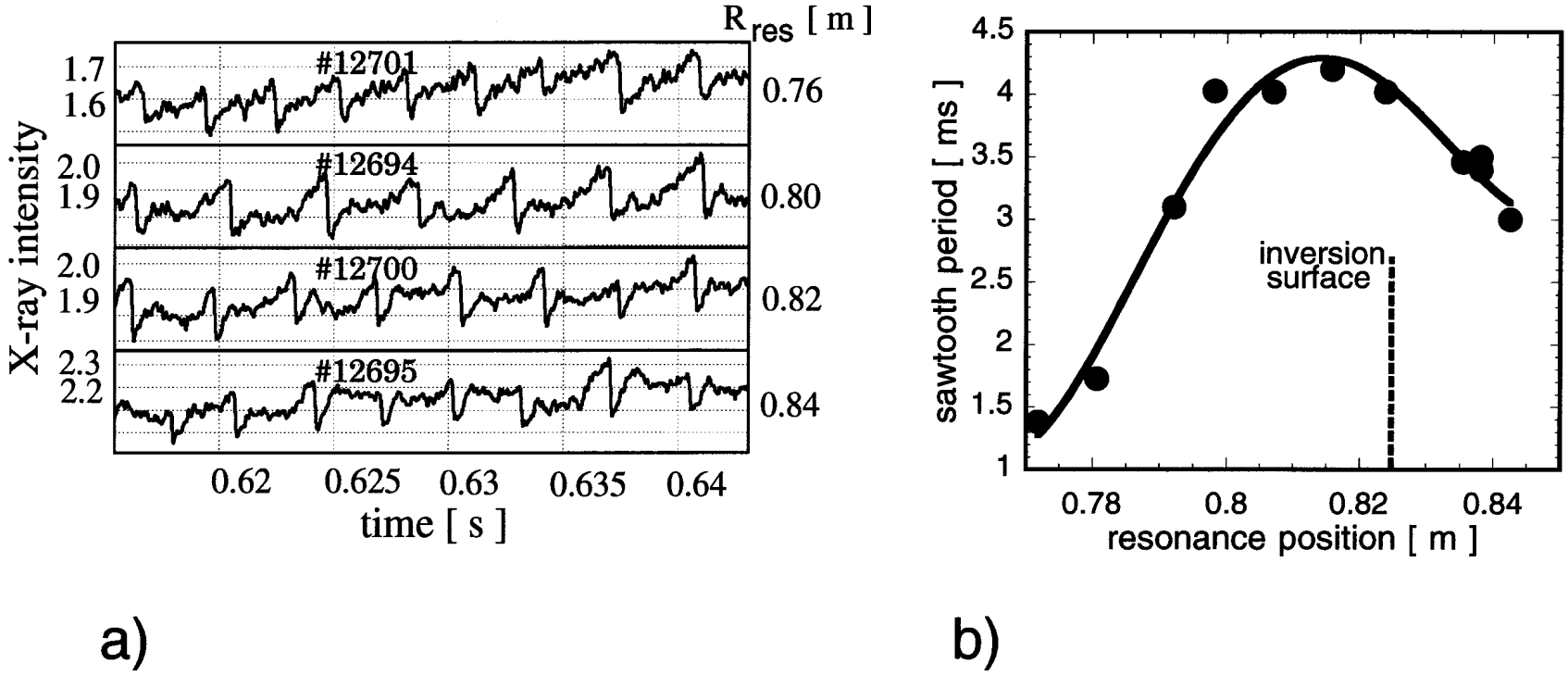

Figure 4. a) Sawteeth activity, and b) sawteeth period modification in a resonance position scan (B_ϕ scan). P_{EC}=360 kW, κ=1.32, $n_e(0)$=2 10^{19} [m^{-3}], q_a=4.7. The position of inversion surface from tomography is R_{inv}=0.825± 0.015 m.

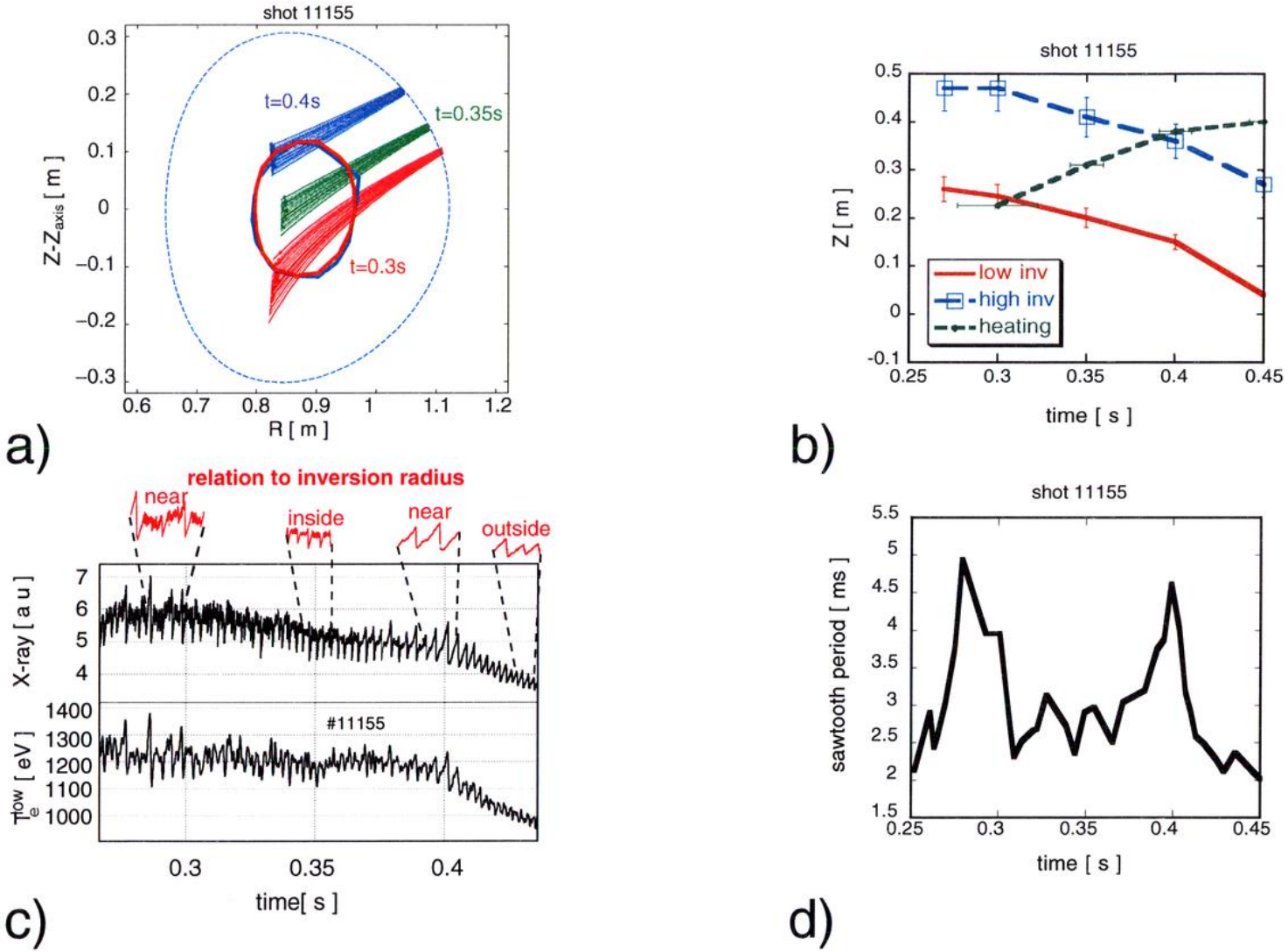

Figure 5. Vertical plasma position sweep: the heating location crosses the bottom part of the inversion surface near t=0.27s, the top part near t=0.4s. There is a noticeable difference in the sawteeth shapes depending on whether power deposition occurs on the upper or lower inversion surface, yet no difference in the sawteeth period: a) inversion surfaces from tomography and beam position from TORAY, b) upper and lower inversion radius and beam position from TORAY, c) soft x-ray flux and soft x-ray temperature, d) sawtooth period maxima for close to inversion radius deposition.

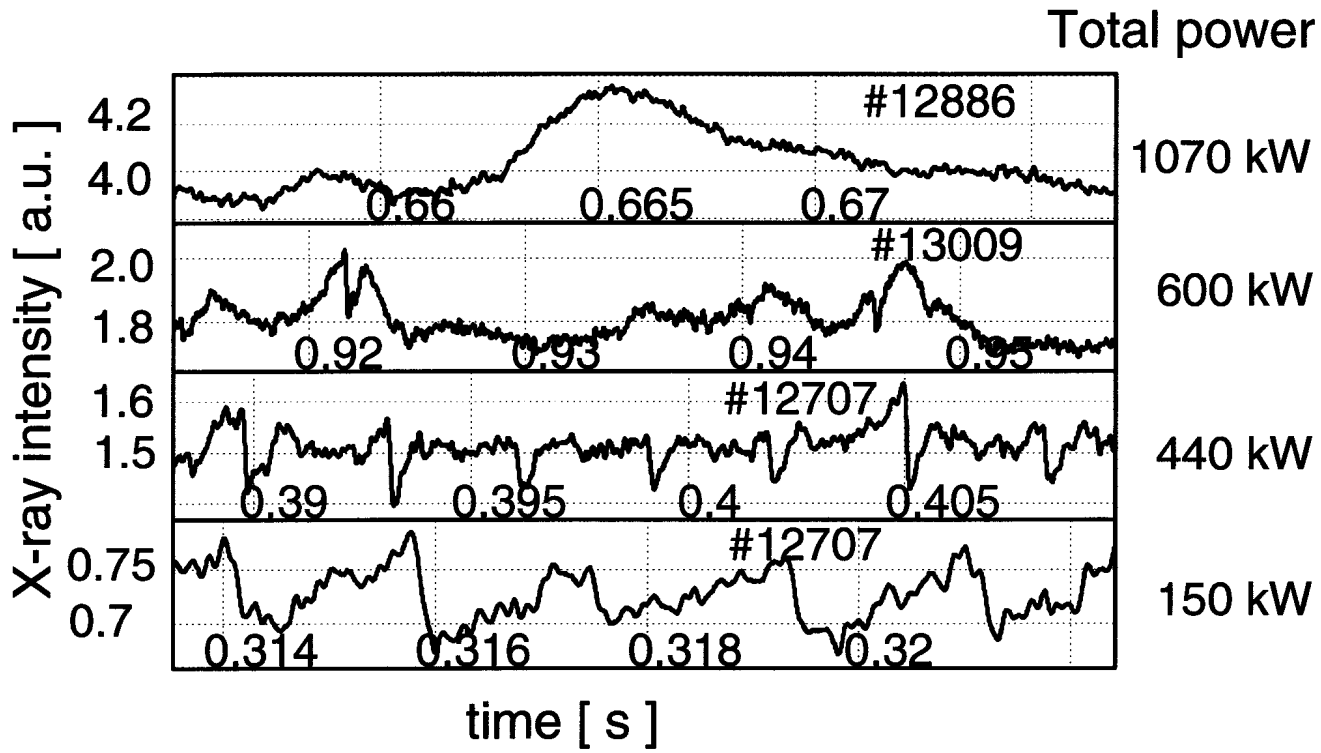

Figure 6. Activity on soft x-rays in a power scan, κ=1.32, q_a=5, $n_e(0)$= 2.2 10^{19} [m^{-3}].

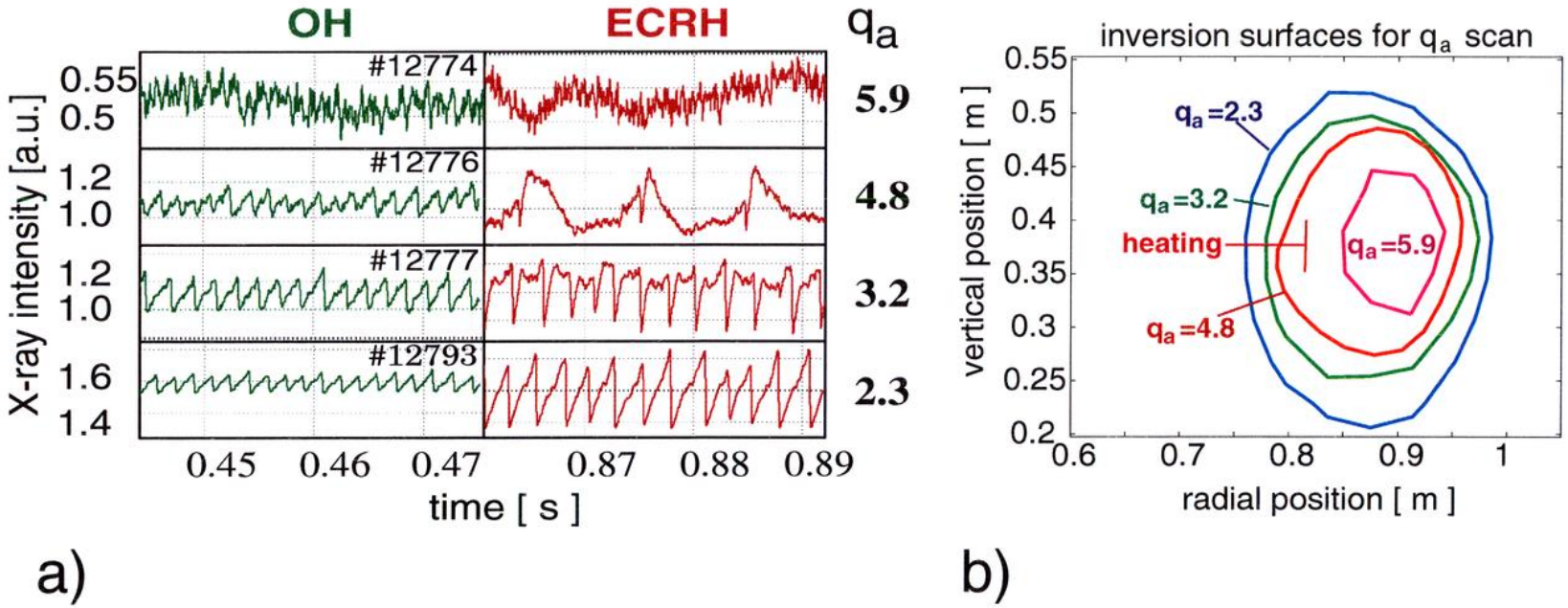

Figure 7 a) Soft x-ray activities as a function of safety factor q_a (κ=1.32, $n_e(0)$=2 10^{19} [m^{-3}], P_{EC}=500 kW). The vertical scales are the same for ECRH and OH for comparison, b) inversion surface from SVD analysis of tomographic reconstruction, resonance location near R=0.82.

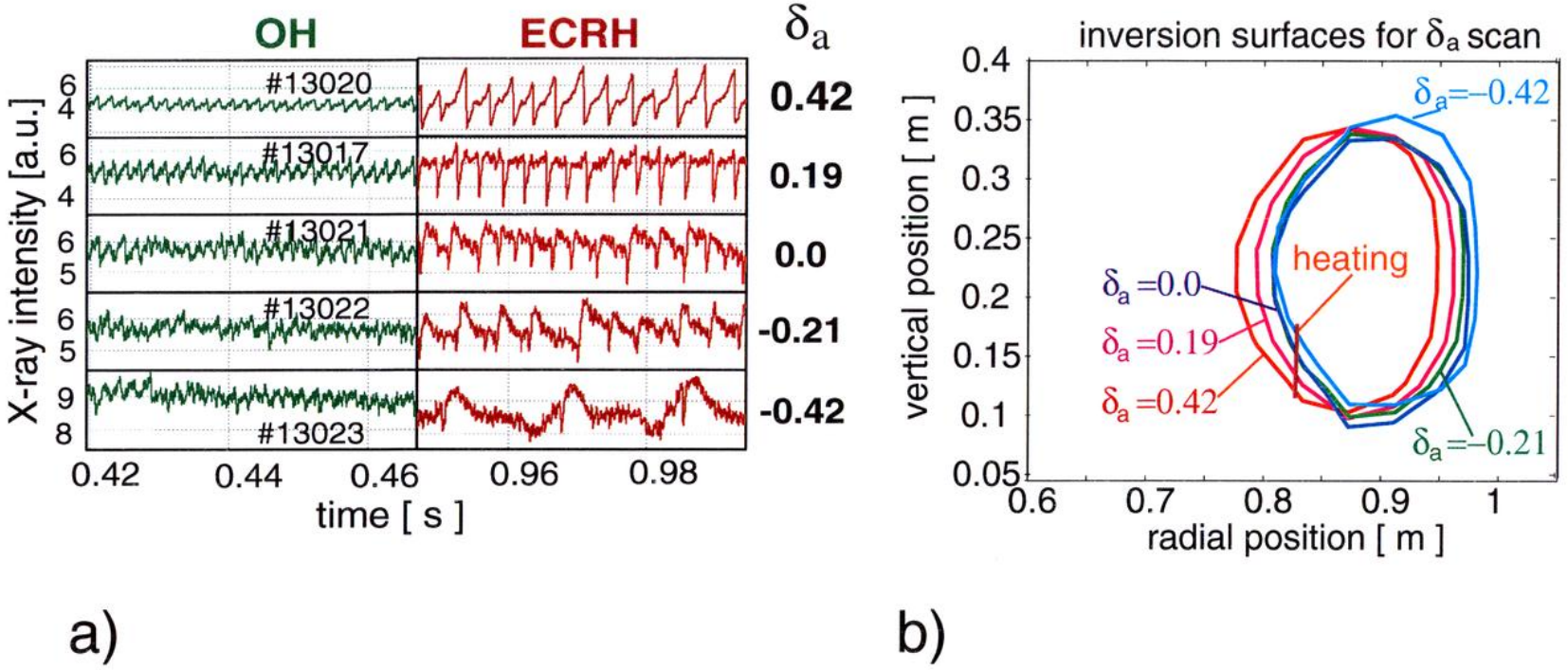

Figure 8. a) Soft x-ray activities in a triangularity scan (κ=1.32, 500 kW, $n_e(0)$=1.8 10^{19} [m^{-3}], q_a=3.5); the vertical scales are the same for ECRH and OH. b) Inversion surface from the SVD analysis of tomographic reconstruction, resonance location near R=0.82 m.

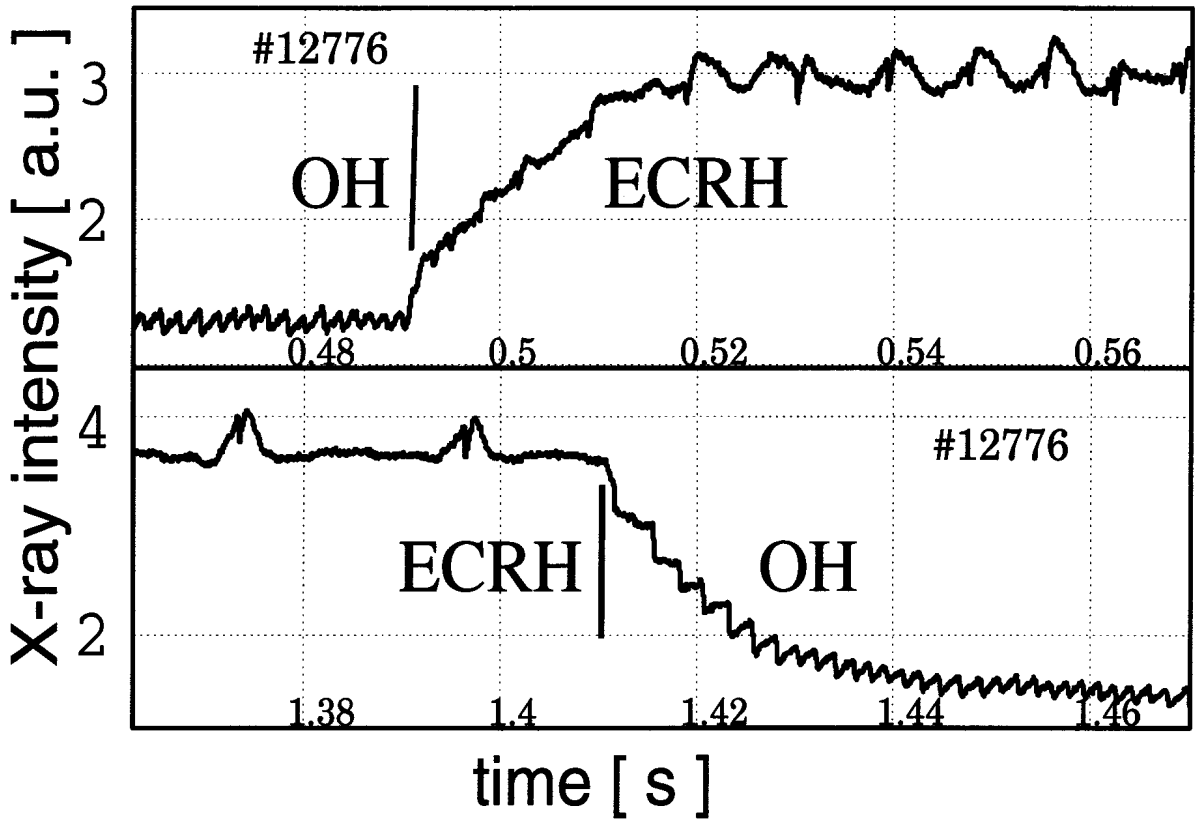

Figure 9. Soft x-ray traces near turn-on and turn-off of ECRH power for a shot exhibiting humpbacks (500 kW, q_a=4.8, $n_e(0) = 2\ 10^{19}$ [m^{-3}]); EC power switching indicated by vertical bars.

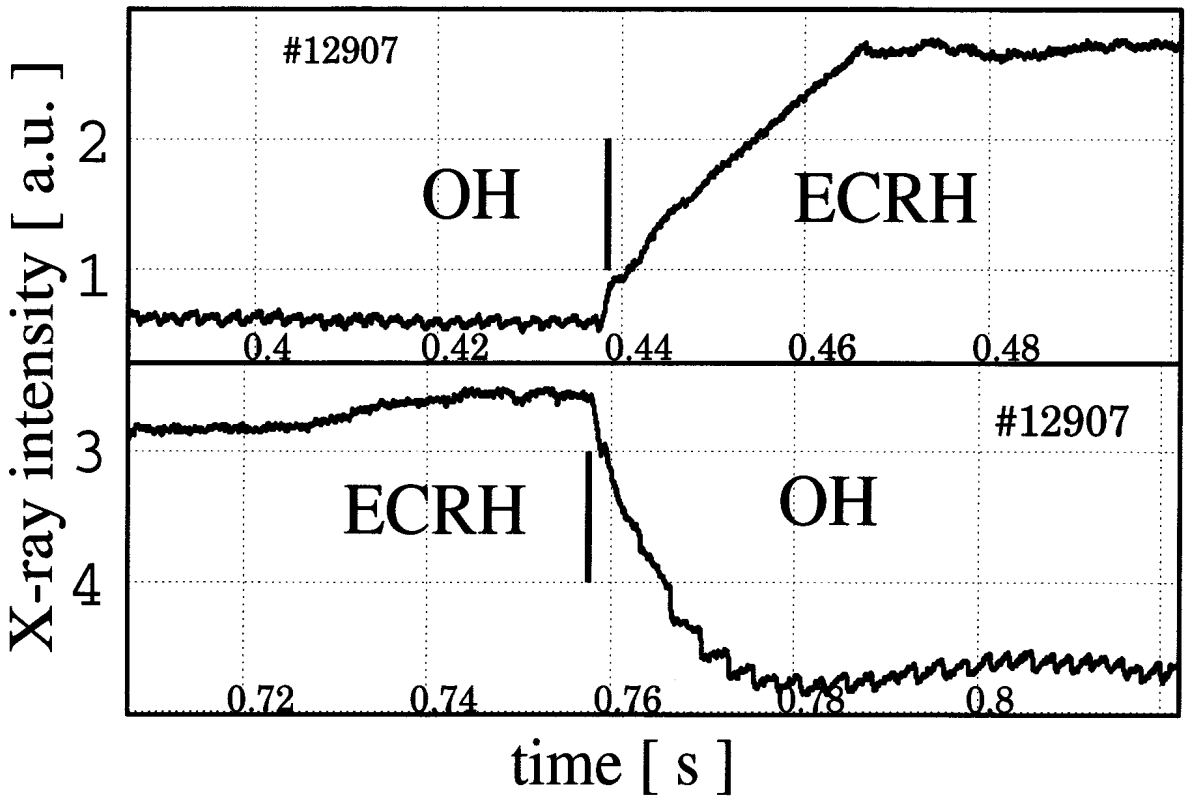

Figure 10. Soft x-ray traces near turn-on and turn-off of EC power for a shot showing very small hills during ECRH (1 MW, q_a=4.7, $n_e(0)$=2 10^{19}[m^{-3}]); EC power switching indicated by vertical bars.

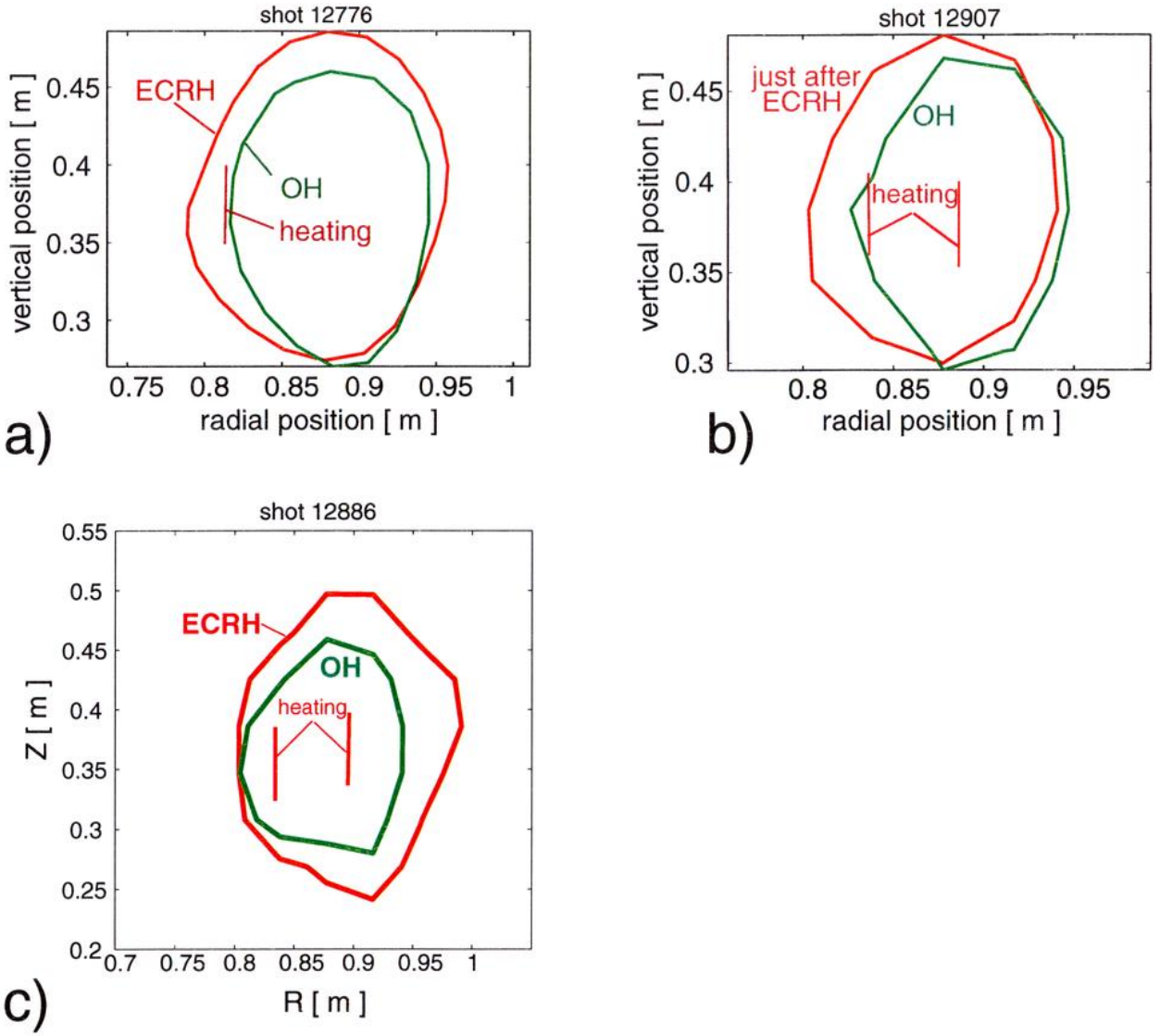

Figure11. a) Humpback sawteeth: heating position relative to inversion surface from tomography during ECRH and OH, b) hills: the inversion surfaces are measured during the first three sawteeth after ECRH (not measurable during ECRH for these small hills) - and during later OH phase.

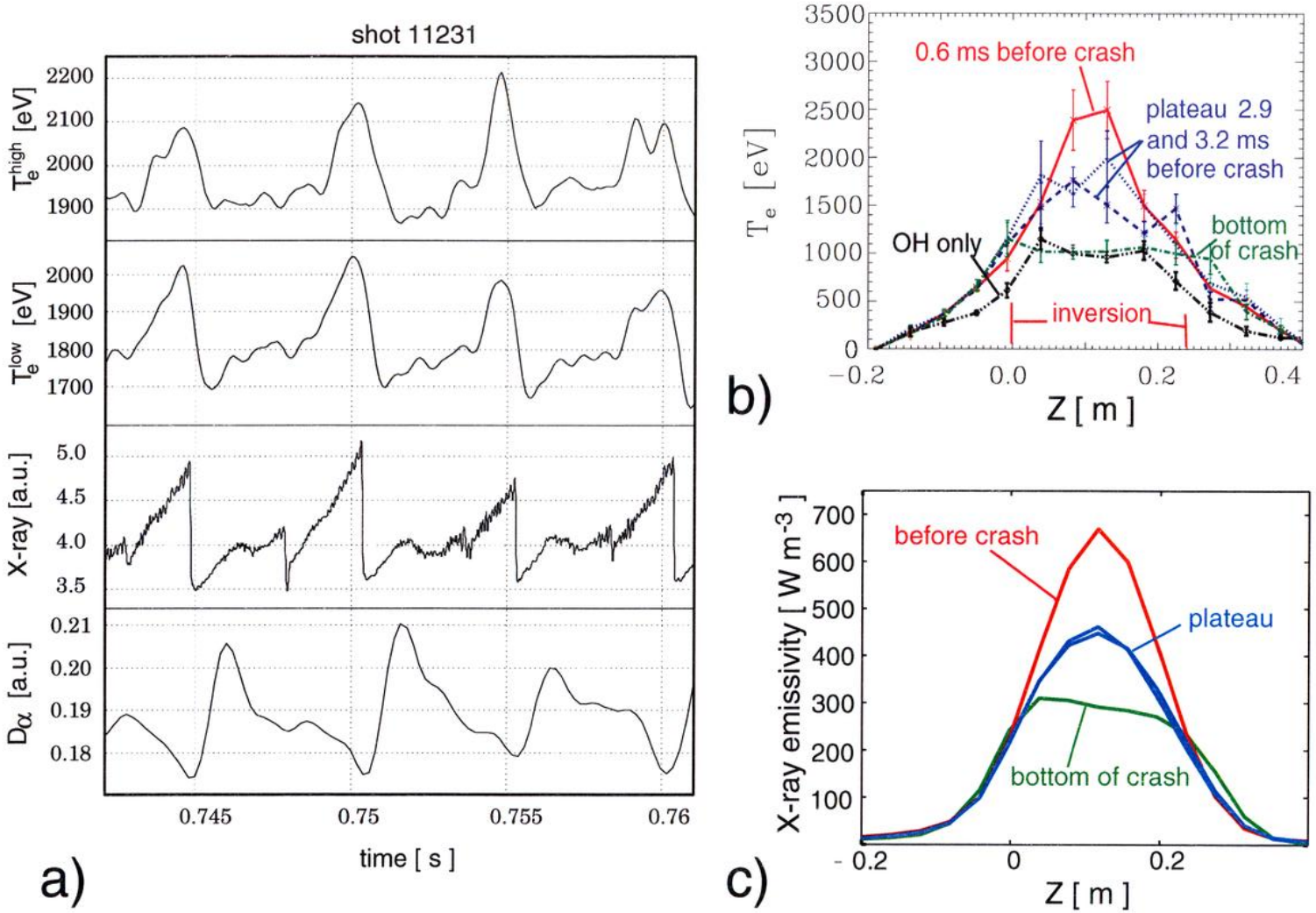

Figure 12. Partially saturated sawteeth: a) "high energy" T_e^{high} and "low energy" T_e^{low} soft x-ray temperature, MHD activity on soft x-ray and D_α signal, b) Thomson temperature profiles; the data are collected from different sawteeth in the same shot and c) soft x-ray profiles from tomographic reconstruction taken at the same time as Thomson profiles. A strong correlation between all signals is shown (q_a=3.5, κ=1.2, 500 kW).

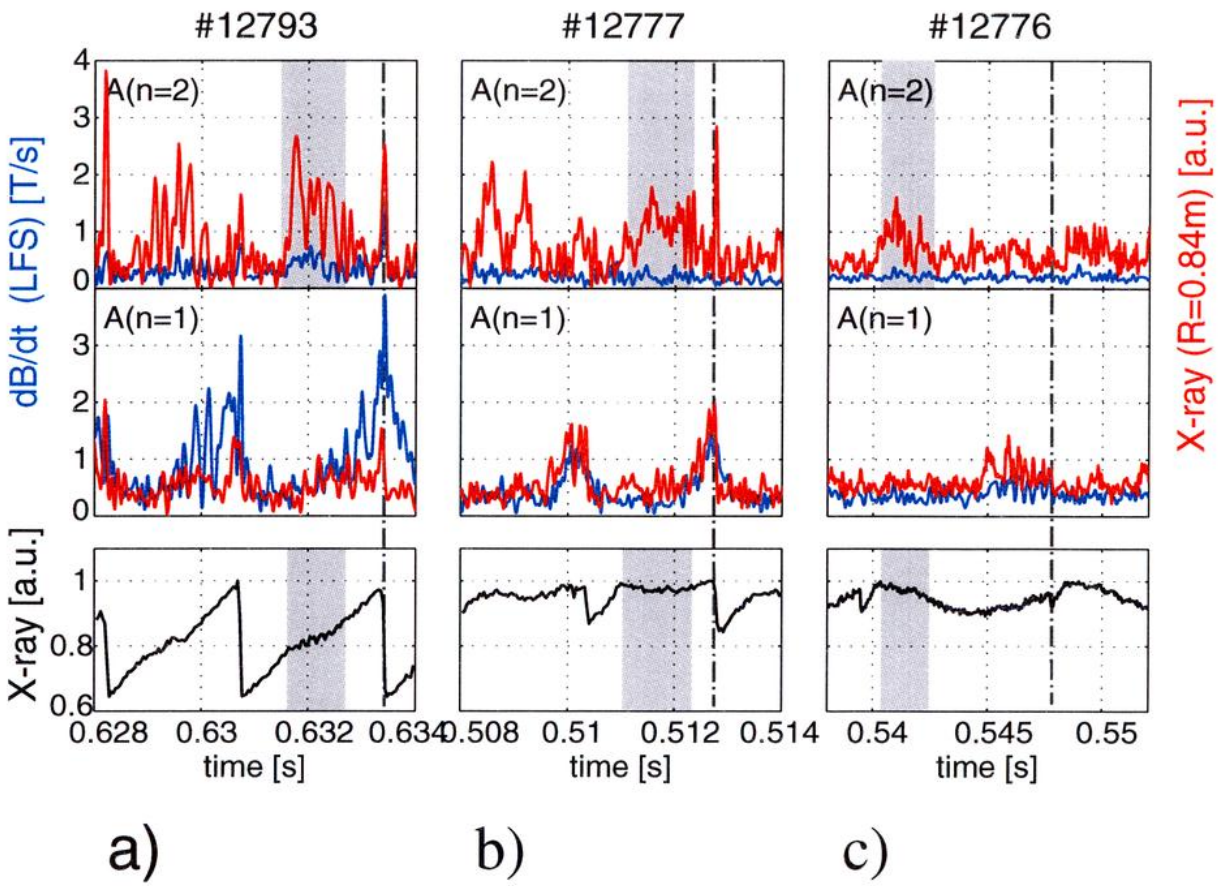

Figure 13. Amplitude of the n=1 and n=2 mode component obtained from magnetic probes at the plasma edge and x-ray intensity along a central chord. Shown are a) partially saturated, b) saturated, and c) humpback sawteeth.

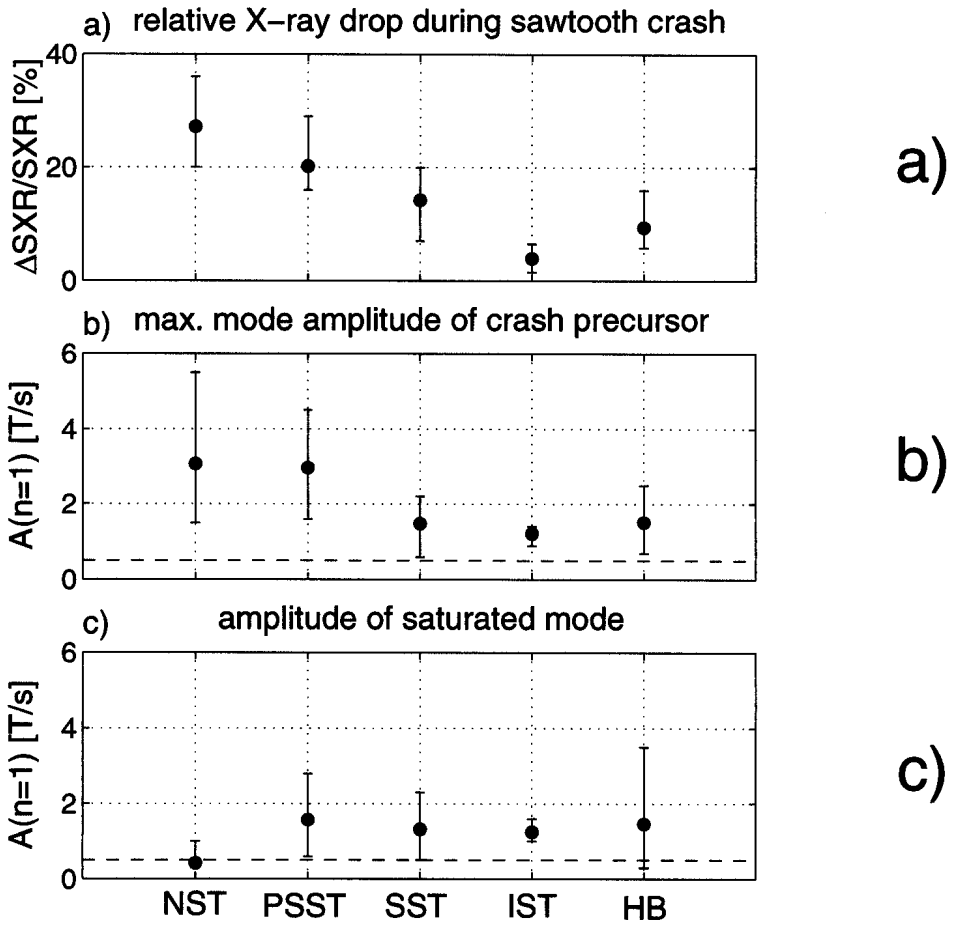

Figure 14. For different types of relaxation: a) central relative X-ray intensity drop at the crash, b) maximum amplitude of the crash precursor, and c) the saturation level of mode activity between crashes are shown. The error bars indicate the maximum and minimum values among the samples (ca. 6 samples/sawtooth type). The dashed line shows the average noise level. NST -normal sawteeth, PSST-partially saturated sawteeth, SST-saturated sawteeth, IST-inverted sawteeth, HB-humpbacks.

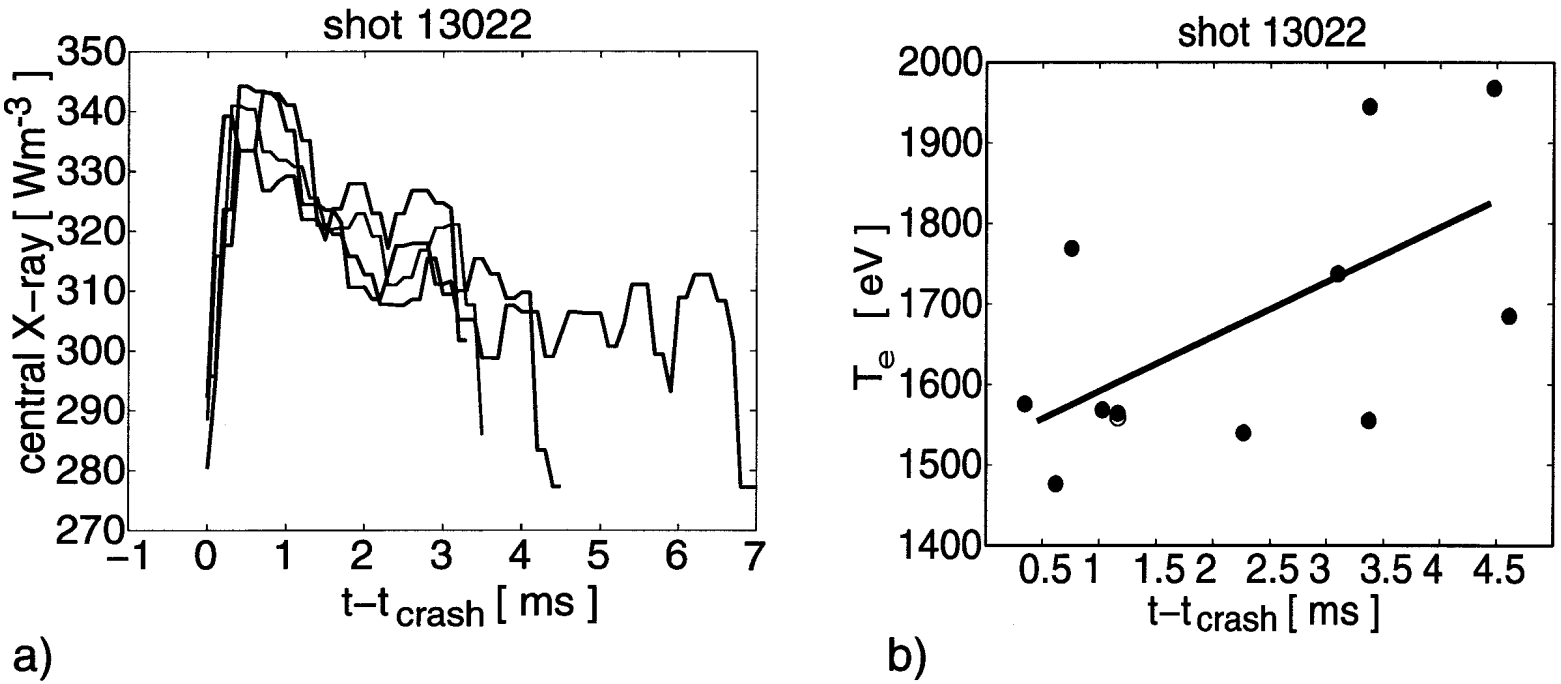

Figure 15. Inverted sawteeth: a) Soft x-ray central emissivity and b) Thomson central temperature, both as a function of time from the nearest sawtooth crash.

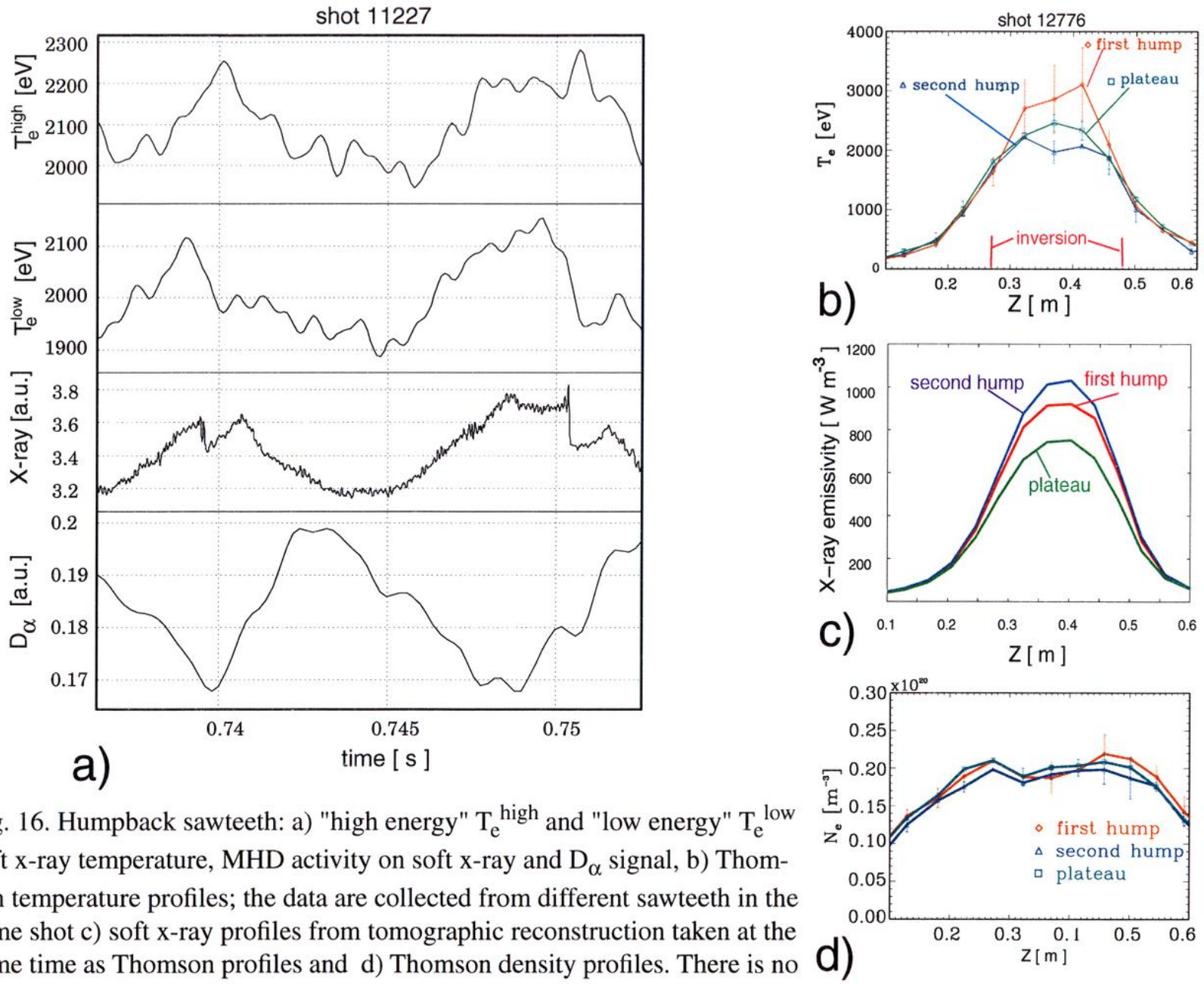

Fig. 16. Humpback sawteeth: a) "high energy" T_e^{high} and "low energy" T_e^{low} soft x-ray temperature, MHD activity on soft x-ray and D_α signal, b) Thomson temperature profiles; the data are collected from different sawteeth in the same shot c) soft x-ray profiles from tomographic reconstruction taken at the same time as Thomson profiles and d) Thomson density profiles. There is no correlation between temperature and X-ray emissivity evolution just after a sawtooth crash (q_a=4.7, κ=1.31, 500 kW).

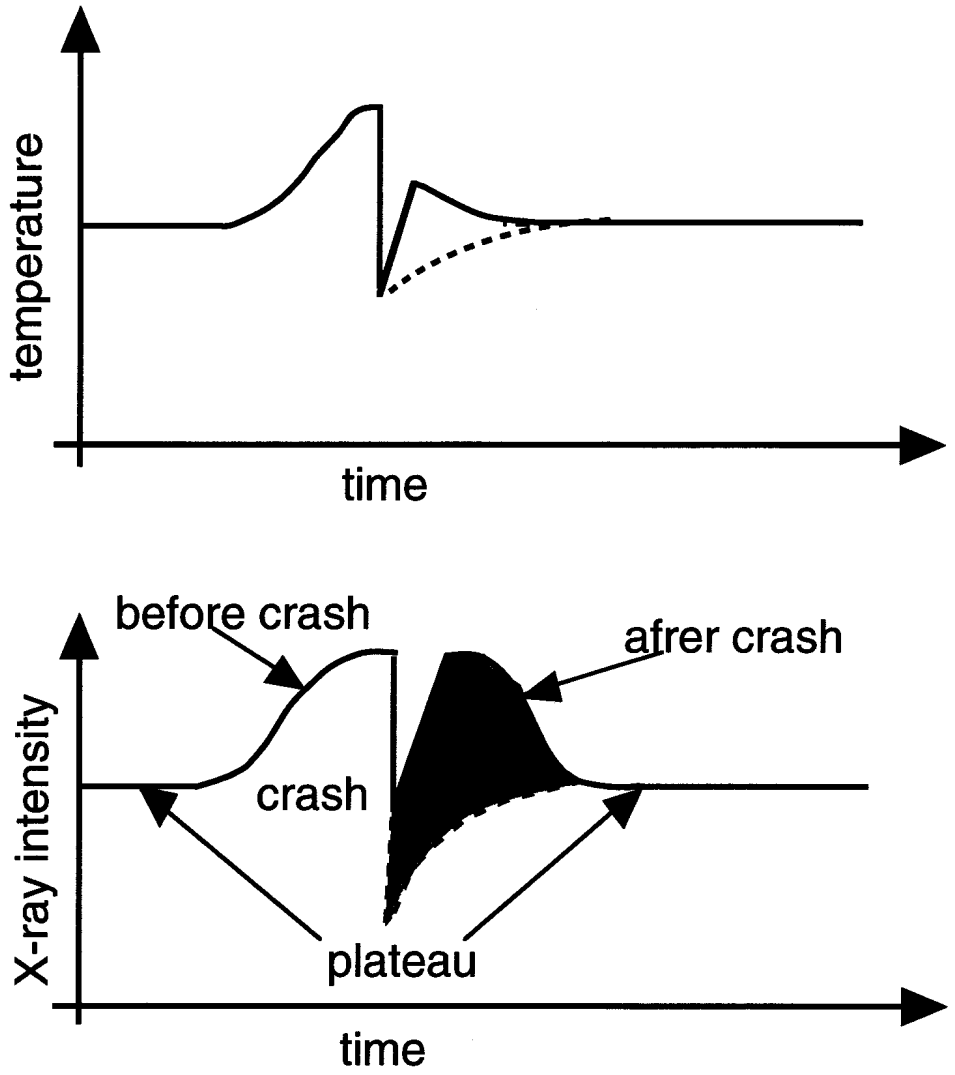

Figure 17 Schematic of the soft x-ray intensity and corresponding temperature behavior during humpback activities.

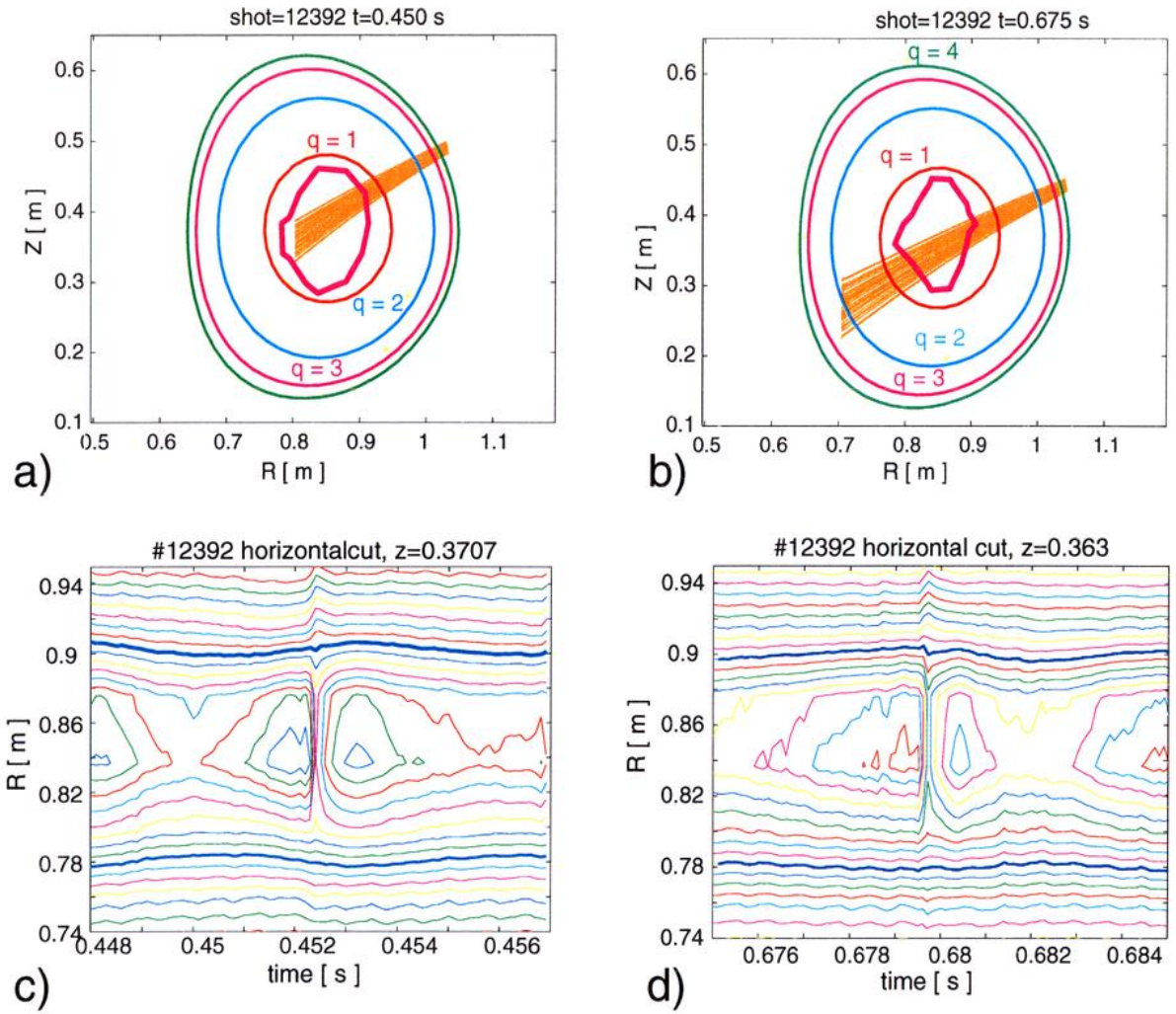

Figure 18. Humpbacks for power deposition at two different radial locations: a, b) Plots of integer q-surfaces from LIUQE equilibrium code, inversion surfaces from tomography and beam position from TORAY for two different times. c, d) Contour plots of x-ray emissivity for corresponding times.

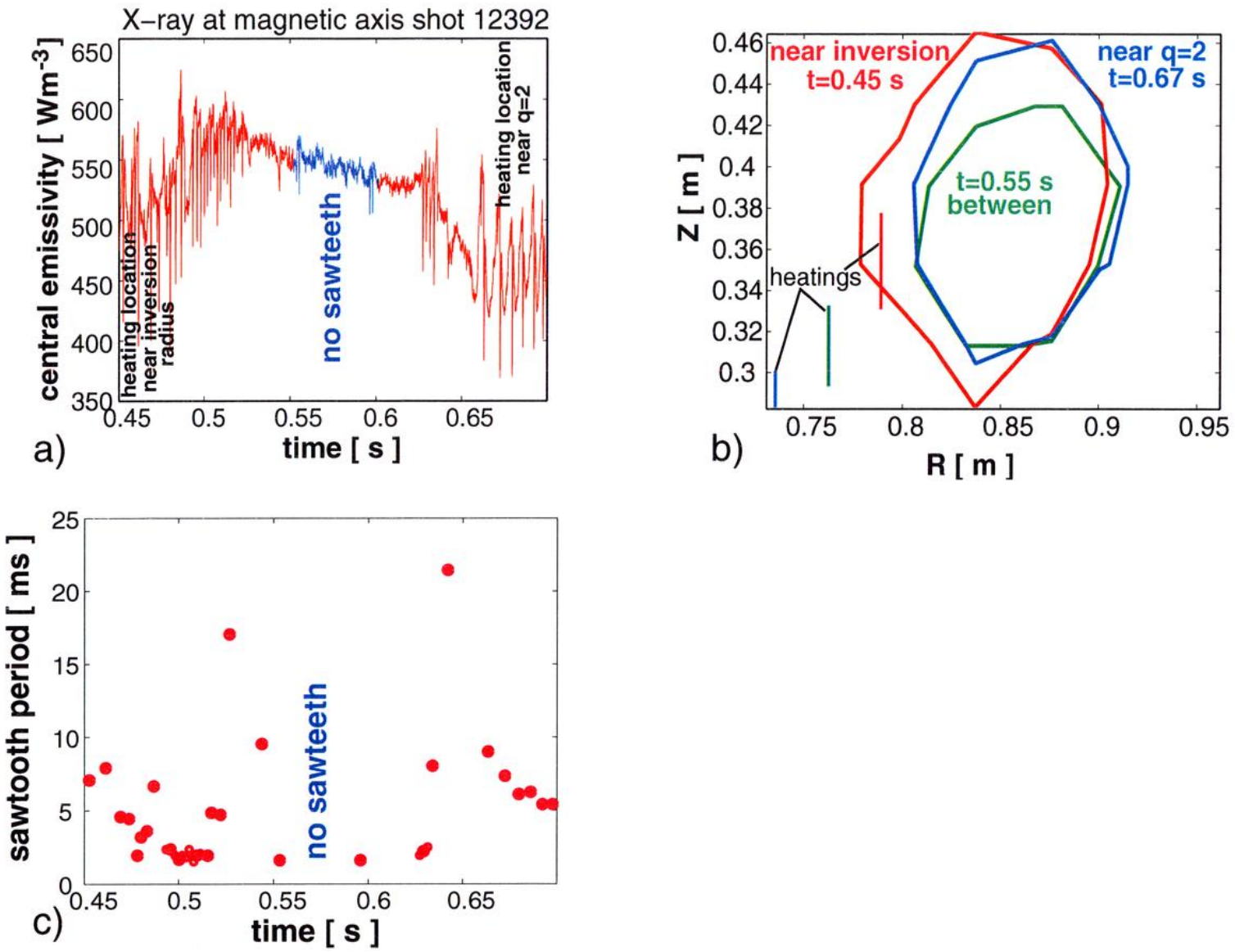

Figure 19. Humpbacks for power deposition at two different radial locations during B_ϕ sweep: a) central soft x-ray intensity, b) inversion surfaces and c) sawtooth period.

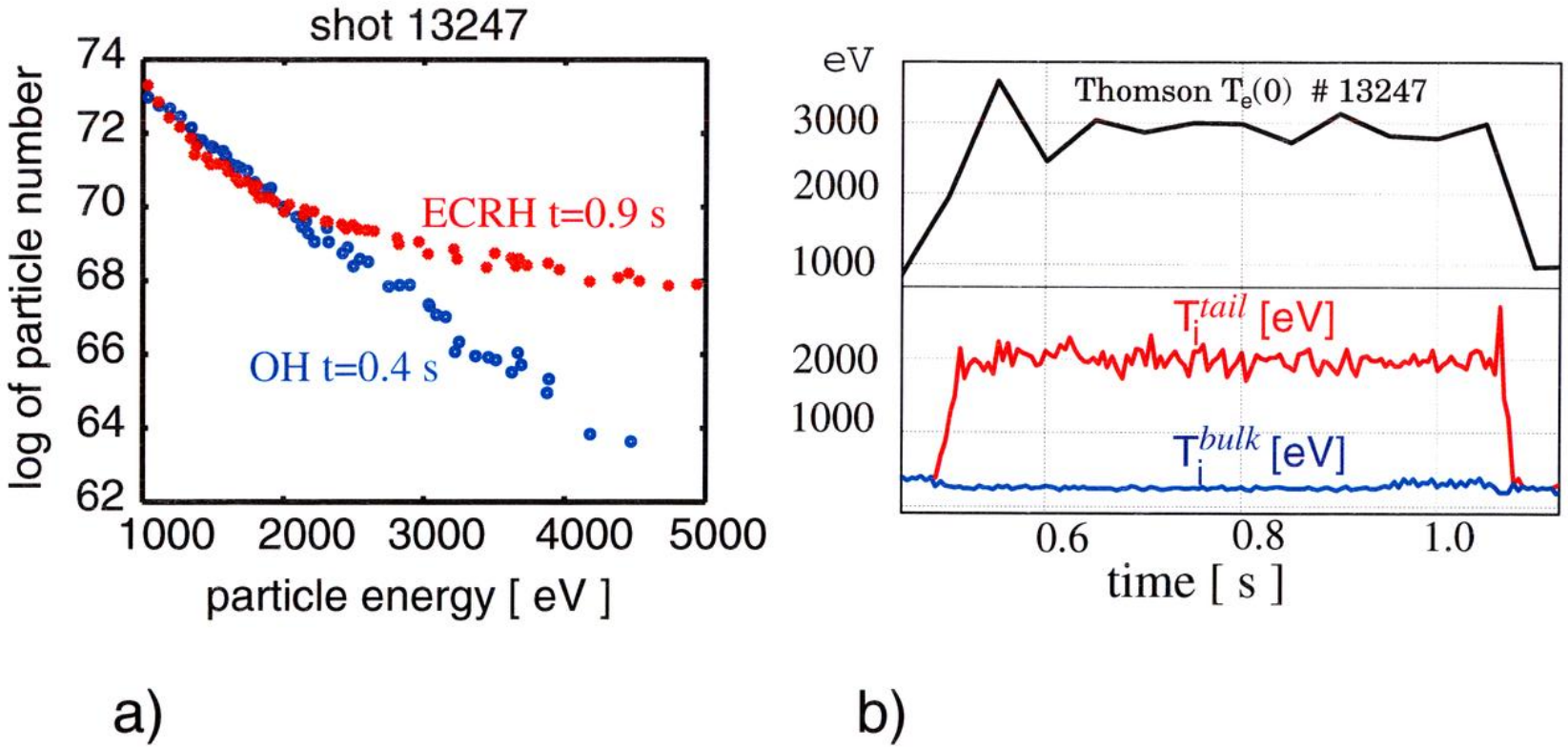

Figure 20. a) Ion energy distribution from Neutral Particle analyzer, b) Central electron temperature, ion "bulk" temperature -blue, and "tail" temperature-red.

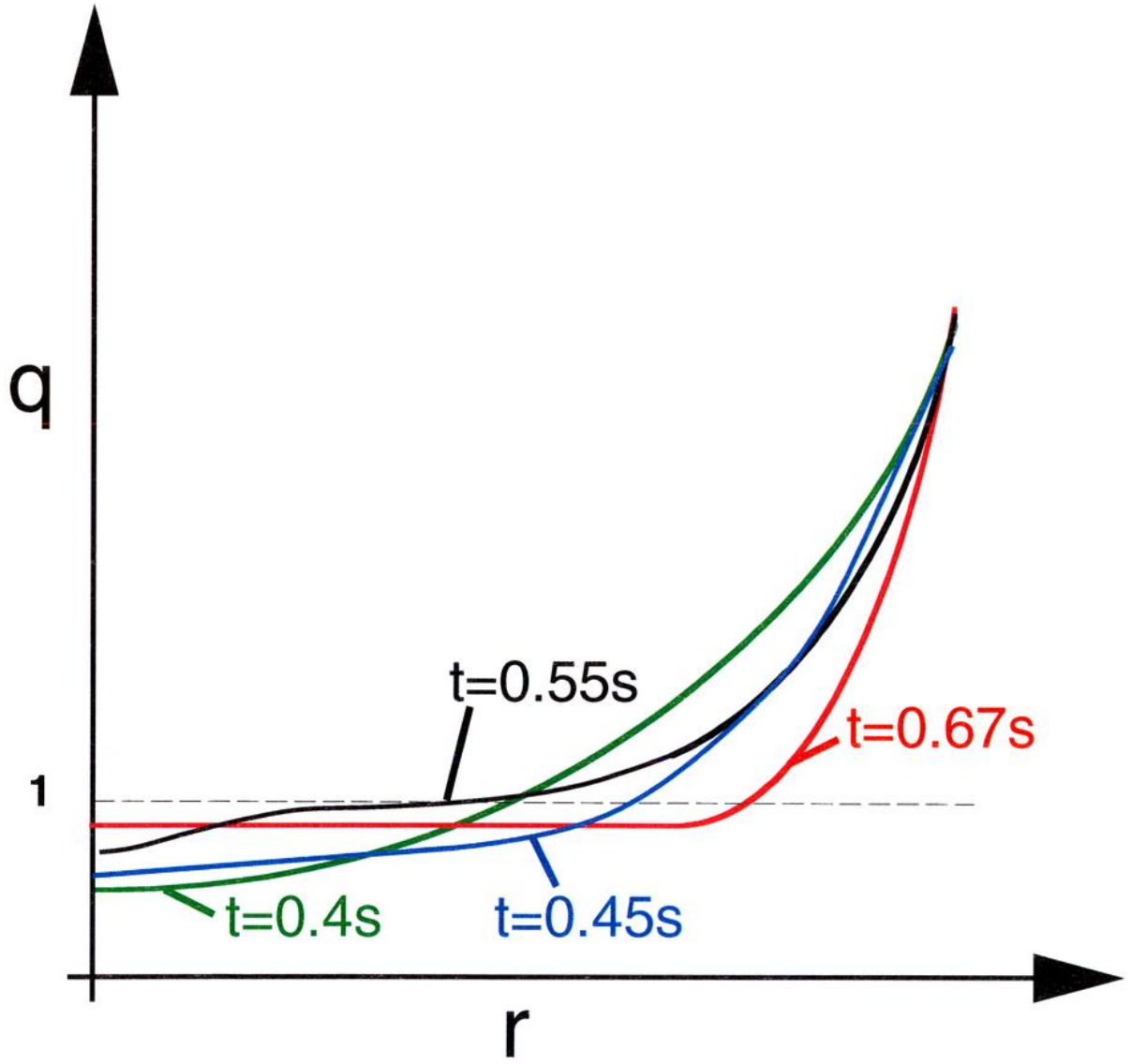

Figure 21. Schematic q-profiles explaining the appearance of large humpbacks for power deposition at two different radial locations.

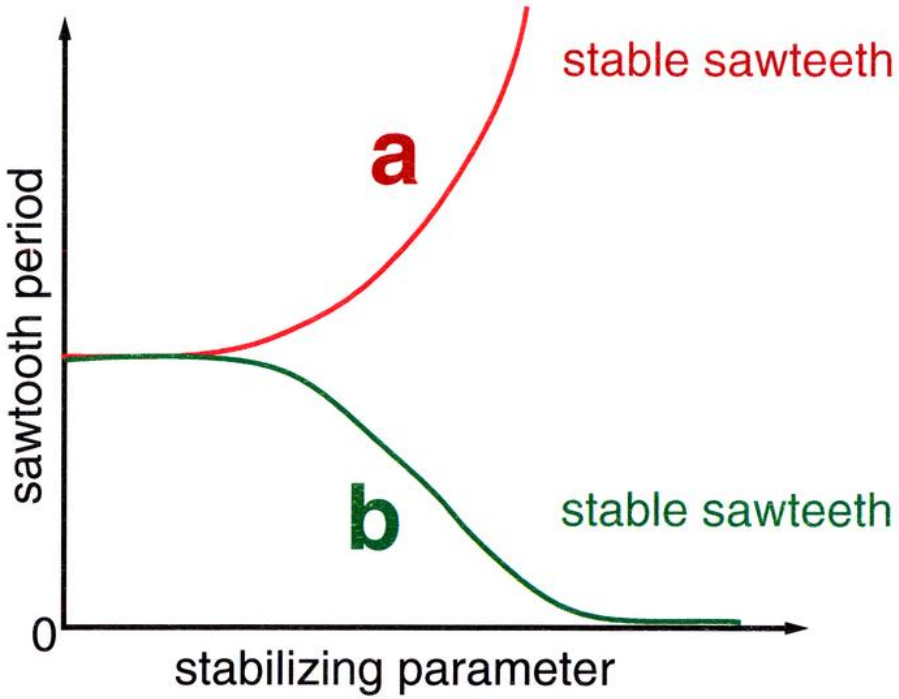

Figure 22. Possible approach to full sawtooth stabilization, by increasing and decreasing sawtooth period.

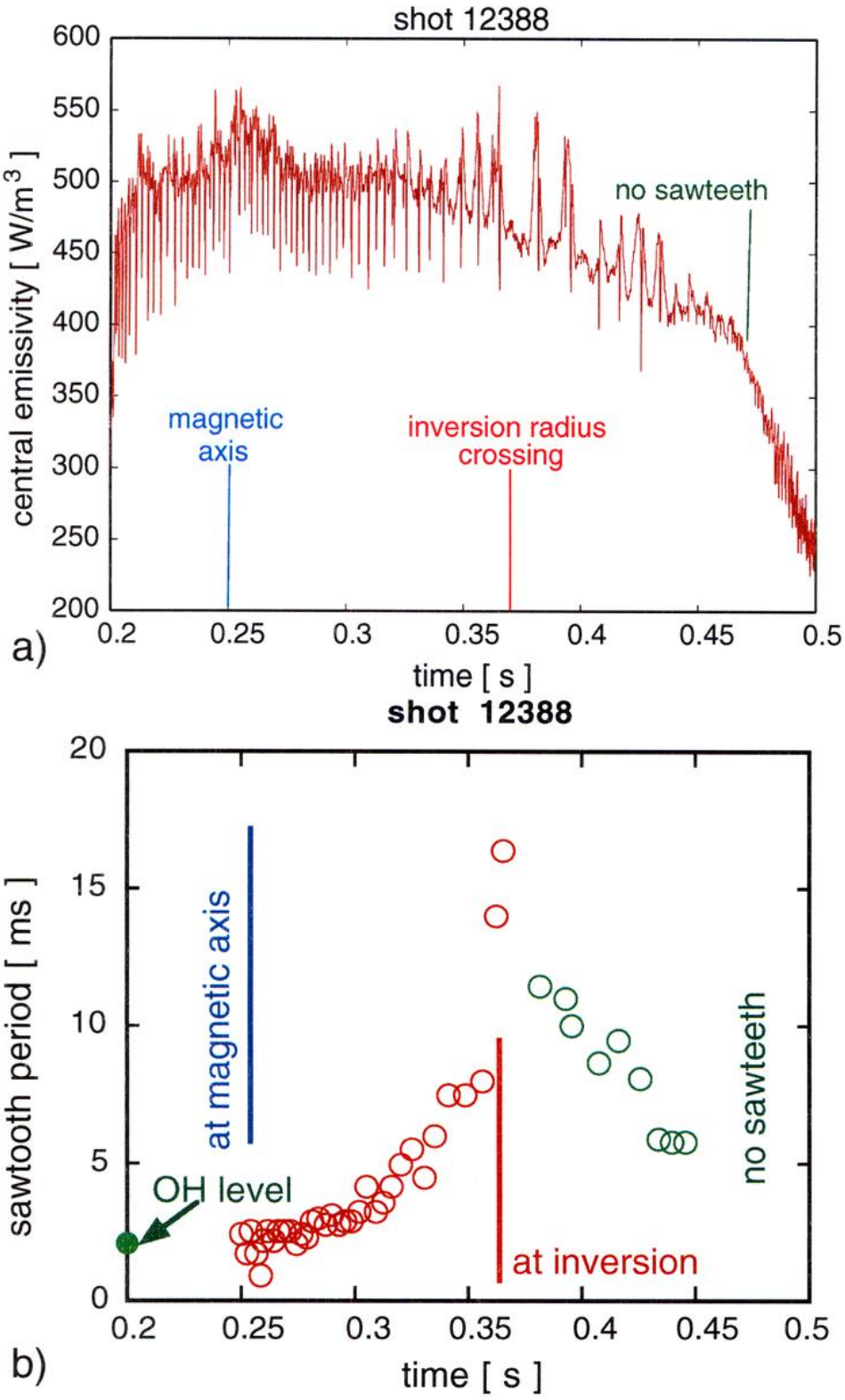

Figure 23. a) Central soft x-ray intensity as a function of time in a B_ϕ sweep for a shot with magnetic axis crossing, b) sawtooth period for the same times.

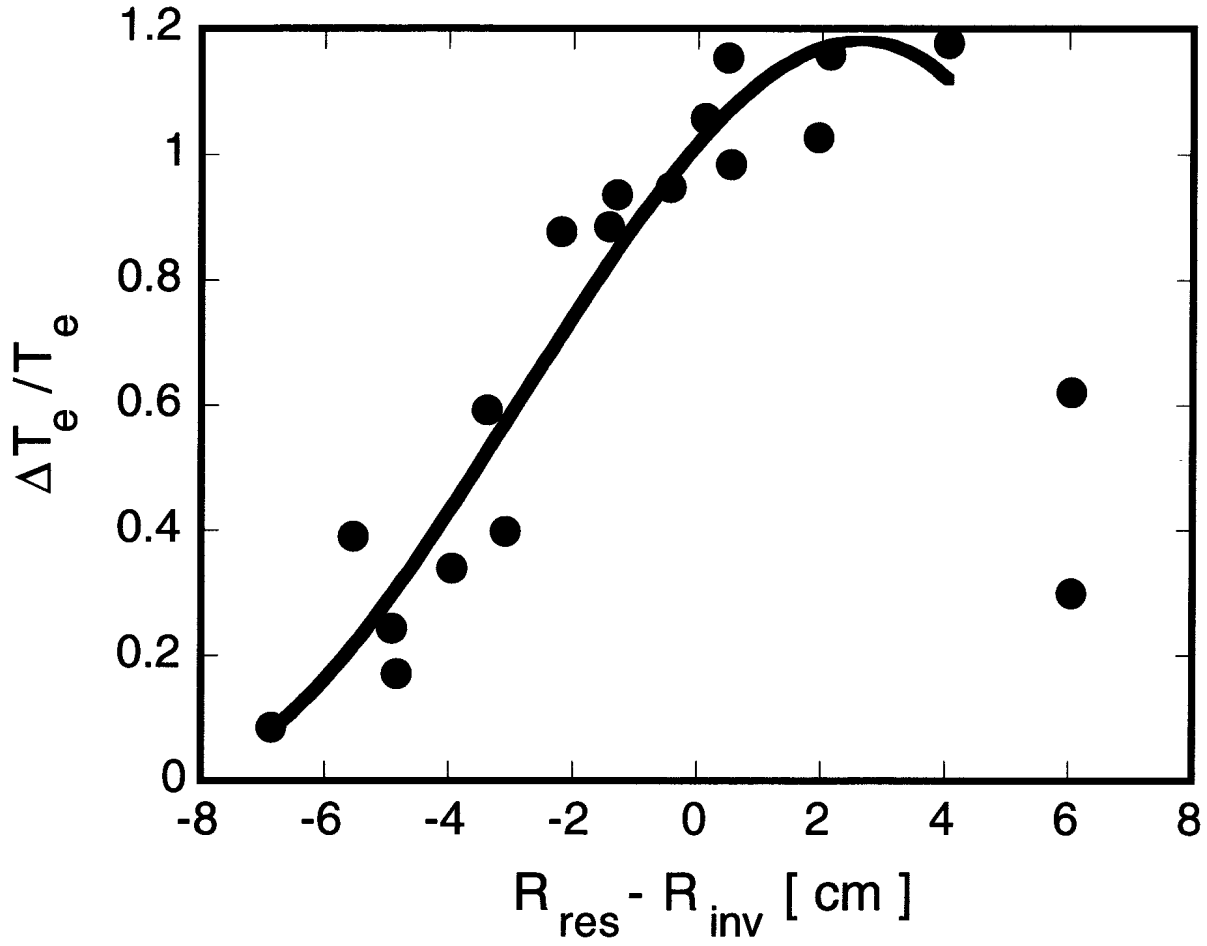

Figure 24. Relative central temperature increase between ECRH and OH as a function of resonance position with respect to inversion surface, P_{EC}=500kW. Data from different resonance positions and q_a. $\Delta T_e/T_e = [T_e(0)_{ECRH}\text{-}Te(0)_{OH}] / T_e(0)_{OH}$

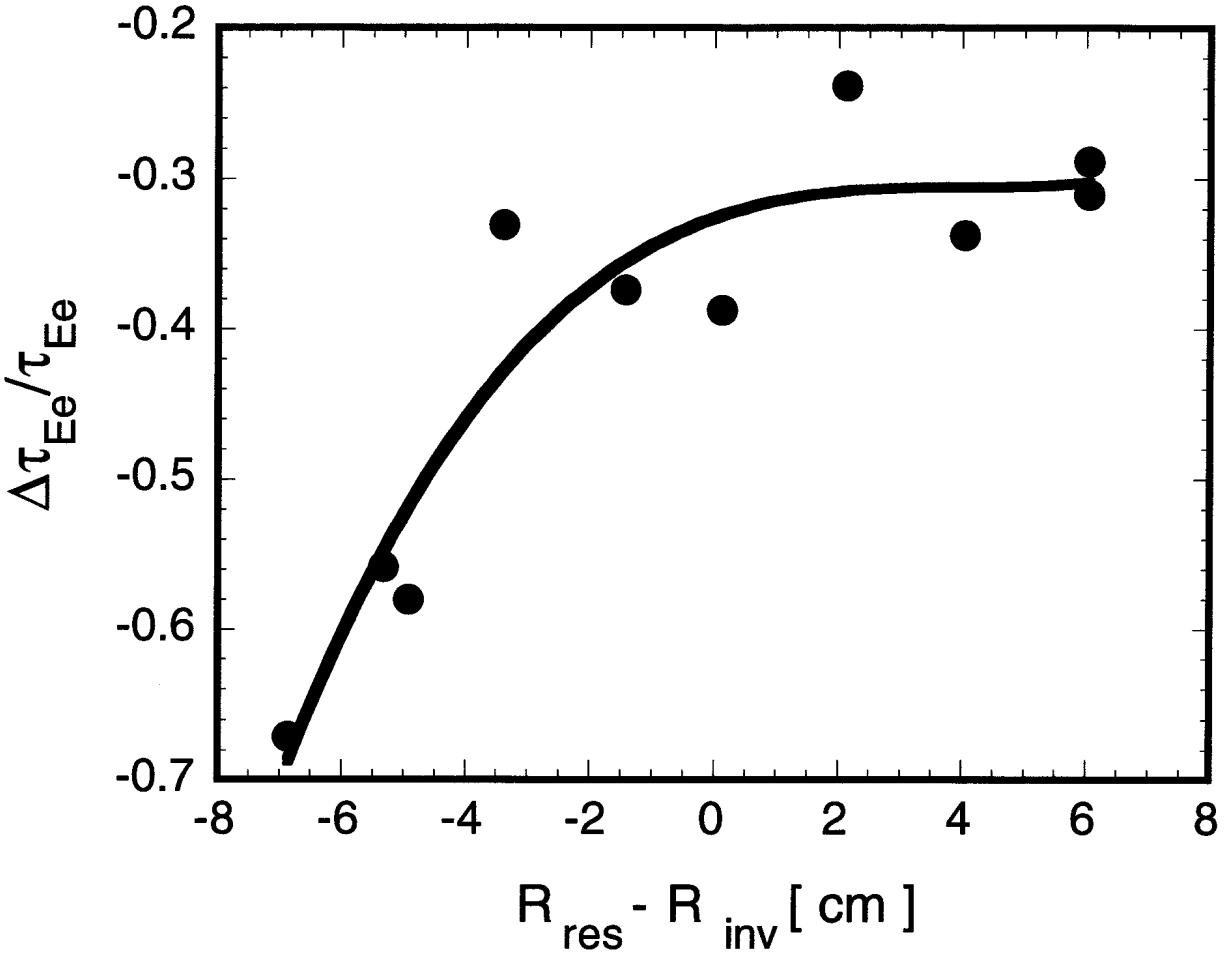

Figure 25. Relative change in global electron confinement time as a function of distance of resonance position with respect to inversion surface, P_{EC}=500kW. Data from different resonance positions and q_a.
$\Delta\tau_{Ee(ECRH)} / \tau_{Ee(OH)} = [\tau_{Ee(ECRH)} - \tau_{Ee(OH)}] / \tau_{Ee(OH)}$

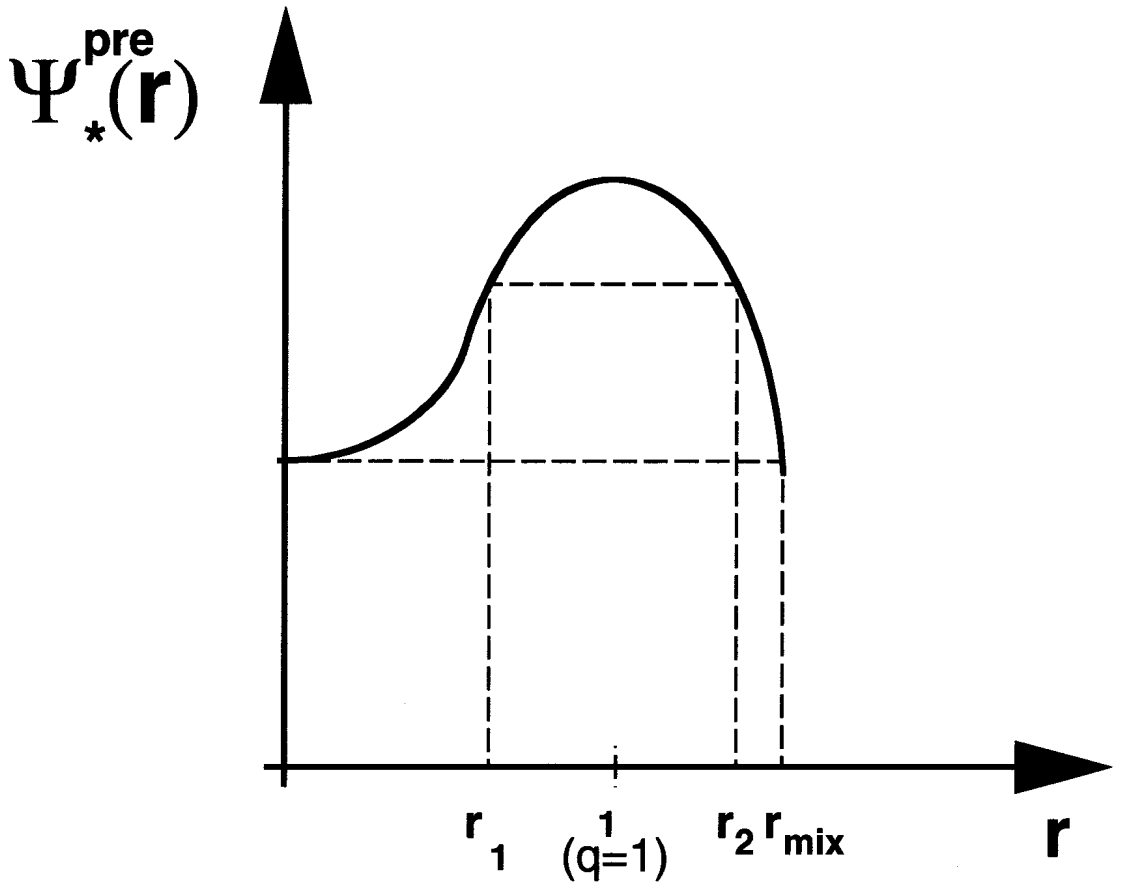

Fig. B1. Schematic of psi profile used in calculation of inversion radius - q=1 relation.